SEVENTH FRAMEWORK PROGRAMME

PROJECT DELIVERABLE

CASPER

CHILD ADVANCED SAFETY PROJECT FOR EUROPEAN ROADS

Grant Agreement number: 218564

Date of latest version of Annex I against which the assessment will be made: 1/09/2010

Deliverable No.	D2.3.2
Deliverable Name	Report on 1Y and 6M child models
Dissemination level	Public

Written By	**Frank MEYER (UdS)** Tel: 00 333 68 85 29 45, meyer@imfs.u-strasbg.fr **Caroline DECK (UdS)** Tel: 00 333 68 85 29 40, deck@imfs.u-strasbg.fr **Carmen RODARIUS & Riske MEIJER (TNO)** Tel : +31 (0)88 8665753 – **riske.meijer@tno.nl** **Jikuang YANG (CHALMERS)** **Tel:** +46 31 7723656**,** jikuang.yang@chalmers.se
Checked by	**Rémy WILLINGER (UdS)** Tel: 00 333 68 85 29 23, willi@imfs.u-strasbg.fr Xavier TROSSEILLE (GIE RE PR) Tel: 00 331 76 87 35 16, xavier.troseille@lab-france.com
Approved by	**Philippe LESIRE (GIE RE PR)** Tel: 00 331 76 87 35 60, philippe.lesire@lab-france.com

Issue date	21 July 2011

CONTEXT / ABSTRACT

This document is the deliverable D.2.3.2 of the CASPER project. It has been done in the framework of WP2 “Child human body modeling” task 2.3 “Develop specific human segments and whole body models per age”.
This task aims to provide the meshing of the whole body models of the 1 year old child (1 Y.O.C.) and six months old child (6 M.O.C).

This document is structured around two sections.

The first part concerns head and neck finite element models development of a 6 M.O.C conducted by UdS as well as a 6 month old multi-body full body human model conducted by TNO.
The new finite element head model simulates closely the main anatomical features: skull, sutures, fontanel, falx, tentorium, subarachnoid space, scalp, cerebrum, cerebellum and brainstem.
The neck model integrates the first thoracic vertebra, the seven cervical vertebrae, intervertebral discs and the upper and lower ligamentary system.
For the 6 month old multi-body full body human model, as base model for the baby model, the TNO’s facet 50th percentile human occupant model was used and scaled down towards baby dimensions using the MADYMO/Scaler. The baby model geometry was based on CANDAT database geometry

The second part of this document aims to present detailed 1 Y.O.C. FEM including a detailed head-neck model provided by UdS and the whole skeleton and the ligaments and flesh attached to them of the other parts developed by CHALMERS.
The starting point of the 1 Y.O.C. model is the DICOM data provided by LMU. The data comes from a 11months 21 days old child with a height of 78cm and weight of 9.6kg.

TABLE OF CONTENTS

1 INTRODUCTION 4

2 6 M.O.C. MODEL 6

2.1 INTRODUCTION 6
2.2 6 M.O.C. HEAD-NECK FEM (UDS CONTRIBUTION) 6
2.2.1 Introduction 6
2.2.2 Meshing of the membranes 6
2.2.3 Meshing of the brain 7
2.2.4 Meshing of the CSF 8
2.2.5 Meshing of the Skull and face 8
2.2.6 Meshing of the scalp 9
2.2.7 6 M.O.C. neck model 10
2.2.8 Conclusion 10
2.3 NUMERICAL FULL BODY 6 M.O.C MODEL (TNO CONTRIBUTION) 12
2.3.1 Method 12
2.3.2 Scaling 12
2.3.3 Most vulnerable body parts 15
2.3.4 Validation 17
2.3.5 Verification 18
2.3.6 Conclusions 22

3 1 Y.O.C. FE MODEL 23

3.1 INTRODUCTION 23
3.2 THE 1 Y.O.C. HEAD MODEL (UDS CONTRIBUTION) 23
3.2.1 Introduction 23
3.2.2 Meshing of the membranes 23
3.2.3 Meshing of the brain 25
3.2.4 Meshing of the CSF 25
3.2.5 Meshing of the Skull and face 26
3.2.6 Meshing of the scalp 27
3.2.7 Conclusion 27
3.3 THE 1 Y.O.C. NECK FE MODEL (UDS CONTRIBUTION) 29
3.4 HEAD AND NECK COUPLING OF THE 3YOC MODEL (UDS CONTRIBUTION) 32
3.5 1 Y.O.C. FE THORAX, ABDOMINAL AND LOWER LEGS MODEL (CHALMERS CONTRIBUTION) 35
3.5.1 Introduction 35
3.5.2 Meshing of the skeleton 35
3.5.2.1 Strategy of remeshing the skeleton 35
3.5.2.2 Cleanup of initial geometry 35
3.5.2.3 Meshing of the long bones 36
3.5.2.4 Meshing of the vertebras 37
3.5.2.5 Meshing of the ribs and sternum 37
3.5.2.6 Meshing of the Scapula and pelvis 38
3.5.2.7 Meshing of the foot and hand 39
3.5.2.8 Summary of mesh layout of whole skeleton model 39
3.5.3 Development of ligaments 39
3.5.4 Development of flesh 40
3.5.5 Development of skin 41
3.5.6 Conclusion 42

4 CONCLUSIONS 43

5 REFERENCES 44

1 Introduction

CASPER project, applied within the framework of the seventh PCRD (FP7-SST-2007-RTD-1) and coordinated by the GIE RE – PSA/Renault (LAB), intends to focus about children and tries to understand collision circumstances as well as dynamic solicitations and injury mechanisms that stem from. The complementary approach of this project will allow finding practical answers for children involved in a transportation mode in order to increase their safety. It results a European collaboration between 15 scientific structures, which will determine parameters to improve child dummies, to determine sociological parameters about transportation conditions and circumstances of an accident, data about potential injured zones etc. in order to offer some answers to increase child safety during a crash.

The subtask 2.3 “Develop specific human segments and whole body model per age” is the most important of the WP2 (Child human body modeling) as the children models are developed per age and per segment.

A previous deliverable D221 “child external and internal geometry for modelling purposes” provided essential information related to children external and internal geometry, main percentile values of several dimensions of the children morphology and mechanical properties especially concerning a 6 M.O.C and a 1 Y.O.C.

The objective of the present document, entitled deliverable D2.3.2 “report on 1Y and 6M child models”, is to present a 6 M.O.C. finite element head-neck model, a 6 month old multi-body full body human model as well as a one year old child finite element model developed in this project in terms of meshing segment per segment.

This document is structured around two sections.

The first part concerns head and neck finite element models development of a 6 M.O.C conducted by UdS as well as a 6 month old multi-body full body human model conducted by TNO.
The new finite element head model simulates closely the main anatomical features: skull, sutures, fontanelle, falx, tentorium, subarachnoid space, scalp, cerebrum, cerebellum and brainstem.
Concerning the neck FEM, a simplified neck was developed just to reproduce a global behavior of this structure in terms of stiffness and mass.
For the 6 month old multi-body full body human model, as base model for the baby model, the TNO’s facet 50th percentile human occupant model was used and scaled down towards baby dimensions using the MADYMO/Scaler. The baby model geometry was based on CANDAT database geometry

The second part of this document aims to present detailed 1 Y.O.C. FEM including a detailed head-neck model provided by UdS. The other parts were developed by CHALMERS, including thorax, pelvis, upper limbs, and lower limbs.
The starting point of the 1 Y.O.C. model is the DICOM data provided by LMU. The data comes from a 11months 21 days old child with a height of 78cm and weight of 9.6kg. The cause of death was an infection. Further details to the source and the anonymisation process were already presented and described in the Deliverable D 2.2.1 “Child external and internal geometry for modeling purposes”. A schematic DICOM data provided by LMU in the CASPER project is given in Figure 1.

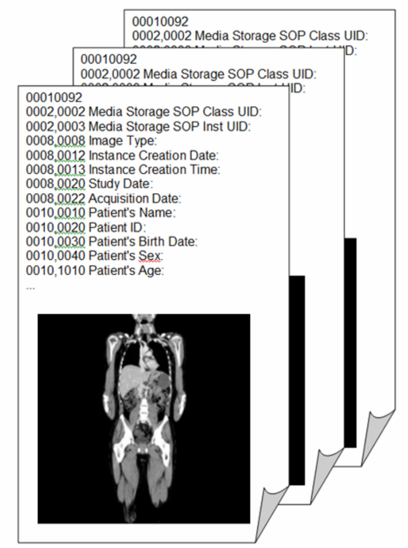

Figure 1. Schematic DICOM data provided by LMU for a 1 Y.O.C.

This 1 Y.O.C. model will be used in order to perform numerical accident simulations and validation in the framework of the task 2.4.

2 6 M.O.C. Model

2.1 Introduction

The first part of this document concerns head and neck finite element models development of a 6 M.O.C conducted by UdS as well as a 6 month old multi-body full body human model conducted by TNO. Results obtained are presented here.

2.2 6 M.O.C. Head-Neck FEM (UdS contribution)

2.2.1 Introduction

The developed finite element head-neck model of a 6 M.O.C. was based on the geometrical 3D reconstruction of slices obtained by CT scanner coming from Strasbourg hospital. Resolution of 2D slices was millimetric. For the reconstruction, 230 slices in transversal plane were used. The scanner sections underwent grey level processing in order to distinguish the bones from the soft tissues. A 3D triangular mesh were then generated and imported in Hypermesh V10.0 software for a step of regular and homogeneous meshing, as needed by explicit codes like Ls-Dyna. An illustration of the segmentation result of the 6 W.O.C. head bones is presented in Figure 2.

In this section, all anatomical features of the 6 M.O.C. head model is presented. Element numbers and quality are reported for each segment (membranes, brain, CSF, skull, face and scalp).

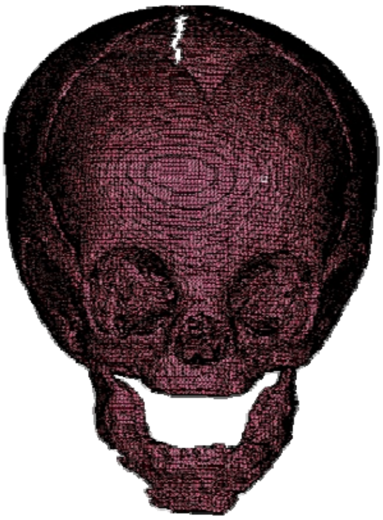

Figure 2. Overview of the segmentation of the 6 M.O.C. external/internal skull and mandibular bones (scans coming from Hautepierre hospital Strasbourg)

2.2.2 Meshing of the membranes

The Falx is a thin arched fold of dura mater which descends vertically in the longitudinal fissure between the cerebral hemispheres. The tentorium is an extension of the dura mater that separates the brain and the cerebellum. The tentorium is an arched lamina, elevated in the middle and inclining downward toward the circumference. It covers the superior surface of the cerebellum and supports the occipital lobes of the brain.

Geometries of these two membranes were defined by using some anatomical atlas and internal skull geometry in order to define tentorium angle.

These thin membranes have been meshed with shell elements with four nodes (quad elements). An illustration of the meshing of these membranes is proposed in Figure 3 (element numbers and quality as computed by the Hypermesh 10 software package (Altair Engineering).

Finally, the falx and tentorium are meshed with 323 and 440 deformable shell elements respectively.

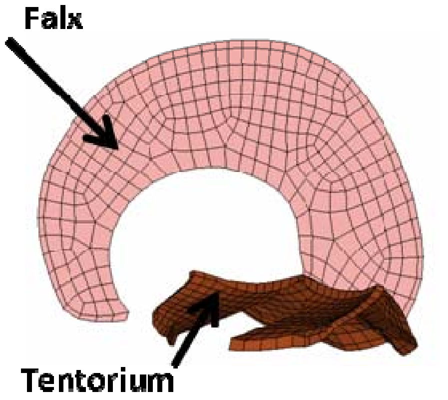

	FALX	TENTORIUM
Type of elements	Shell (quad)	Shell (quad)
Nb of elements	323	440
Max. warpage	0.0026	30.89
Max aspect ratio	4.46	4.38
Min length (mm)	1.25	0.84
Min jacobian	0.52	0.53
Min angle (°)	50.93	28.33
Max angle (°)	140.96	157.48

Figure 3. Overview of brain membranes (falx and tentorium) and mesh characteristics

2.2.3 Meshing of the brain

A special attention was given to the brain and cerebellum meshes to avoid very small elements and elements with very small or big angles that could lead to zero or negative volumes during simulations and unacceptable time steps. It was decided to use hexahedral elements.
Element numbers and quality as computed by the Hypermesh V10.0 software package (Altair Engineering) are summarized in Figure 4.

Finally, the brain and cerebellum are meshed with 10 708 brick elements; an overview of this segment is reported in Figure 4.

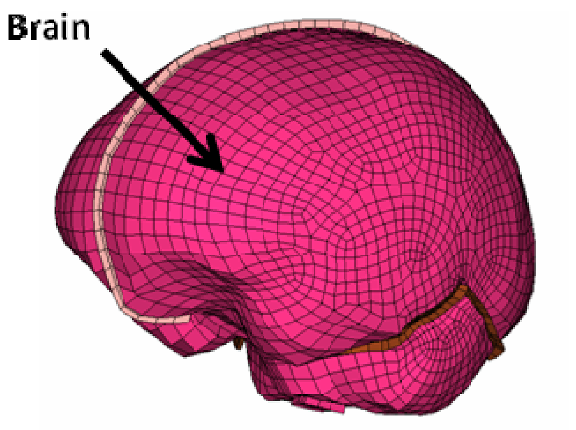

	BRAIN
Type of elements	Solid
Nb of elements	10 708
Max aspect ratio	8.87
Min length (mm)	0.63
Min jacobian	0.18
Min angle (°)	38.61
Max angle (°)	92.33

Figure 4. Overview of brain and mesh characteristics

2.2.4 Meshing of the CSF

The subarachnoid space was modeled between the brain and the skull to simulate the CSF. This space is constituted by a layer of brick elements and it entirely surrounds the brain and membranes (falx and tentorium). For this, a continuous meshing between membranes and brain was applied in order to define CSF. It's an important point to reduce time step which could be appeared by creating interfaces.

Element numbers and quality are summarized in Figure 5.

The CSF is meshed with 4116 brick elements.

	CSF
Type of elements	Solid
Nb of elements	4116
Max aspect ratio	7.69
Min length (mm)	0.82
Min jacobian	0.24
Min angle (°)	38.91
Max angle (°)	92.33

Figure 5. CSF mesh characteristics

2.2.5 Meshing of the Skull and face

The first and main particularity of children head is the fact that the skull is made by bone elements connected by sutures which are not ossificated. The young child sutures are more or less wide and correspond to a fibrous cartilaginous material with very low elastic properties.
The fontanels will progressively ossificate up to approximatively 18 to 36 months old. The most important fontanel is the frontal one (or bregma) with a 2 to 3 cm width. Its diamond shaped and connects three sutures, the coronal suture, the inter-parietal suture and the metopique suture. Its total ossification appears at 15 to 18 months old.
The posterior fontanel (or lamdoïde) corresponds to the junction of the two parietal bones and the occipital bone. This fontanel is much smaller than the previous one with only 0.5 cm in width. It also disappears much earlier at around 2 to 3 months old.
The sphenoid one closes at around 6 months old and the mastoïdian (or asterique) one at 18 months old.

Finally the child has, as the adult, a total of 5 sutures:

- The sagittal suture
- The coronal suture
- The lamdoïd suture
- Two sphenoïdal sutures

The skull is modeled by one layer of shell elements representing the cranial bone constituted by only cortical bone for a 6 M.O.C. Coronal, sagittal, lambdoid and temporo-parietal sutures were modeled with shell elements as well as anterior fontanel. A special attention will be paid on mechanical properties of this skull in order to be able to reproduce skull failure which is an injury mechanism at this age.

A simple face was meshed with shell elements and will be considered as rigid during simulation. This face declared as rigid body will permit to take into account its inertia and mass in the model.

Finally, the skull (including sutures and fontanelle) and the face are meshed with 2816 and 498 deformable shell elements respectively, an overview of these segments are reported in Figure 6.

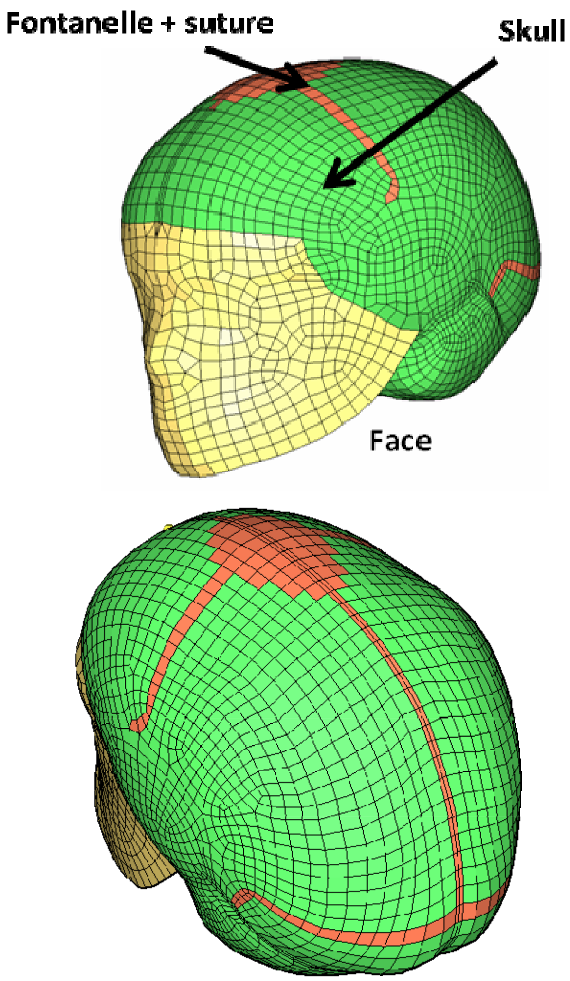

	SKULL+SUTURES	FACE
Type of elements	Shell	Shell
Nb of elements	2816	498
Max. warpage	32.29	29.26
Max aspect ratio	10.94	4.17
Min length (mm)	0.46	1.36
Min jacobian	0.45	0.56
Min angle (°)	22.79	46.87
Max angle (°)	160.48	140.38

Figure 6. Overview of bones (skull, sutures and face) and mesh characteristics

2.2.6 Meshing of the scalp

The scalp was modeled by a layer of brick elements and surrounds the skull and facial bones. A continuous meshing between skull + face and scalp was realized by extruding bones elements. An overview of scalp and mesh characteristics are given in Figure 7. The scalp is meshed with 2602 brick elements.

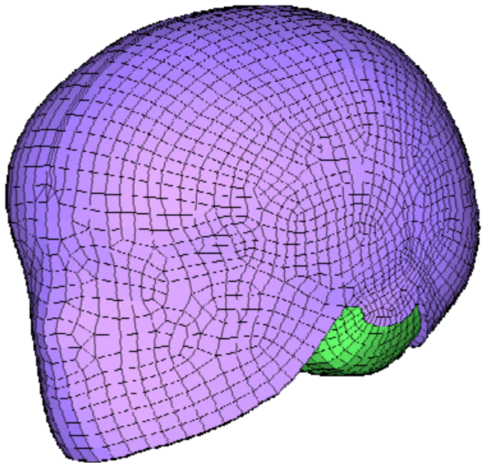

	SCALP
Type of elements	Solid
Nb of elements	2602
Max aspect ratio	7.4
Min length (mm)	0.85
Min jacobian	0.4
Min angle (°)	24.45
Max angle (°)	154.86

Figure 7. Overview of scalp and mesh characteristics

2.2.7 6 M.O.C. neck model

Concerning the neck model at this age the bone process is not finish i.e. it's impossible to distinguish the cartilage to the bone part. Moreover at 6 month a child cannot naturally maintain his head. It is the raison why it has been decide to modelize the neck by a simple column of brick elements wish respect the neck dimension. The objective is to reproduce a global behavior of this structure in terms of stiffness and mass in order to have the correct head kinematics. The average neck length of 6 MOC is 5.3 cm (Schneider et al 1986).

2.2.8 Conclusion

The proposed finite element head-neck model of a 6 M.O.C. head was based on the geometrical 3D reconstruction of 2D slices obtained by CT X-Ray for the head (scanner coming from Strasbourg hospital) and on a simple neck.
For the head, 3D triangular mesh was then generated in STL format and imported in Hypermesh V10.0, allowing regular meshing of the whole head required by explicit codes like Ls-Dyna.

The new finite element head model simulates closely the main anatomical features: skull, sutures, falx, tentorium, subarachnoid space, scalp, cerebrum, cerebellum and brainstem. Concerning the neck it was modelized by a simple tube in order to reproduce the stiffness of the neck for this age.
Figure 8 illustrates the different parts of the developed model.

The finite element mesh is continuous and represents a 6 M.O.C. head-neck model. Globally, the 6 M.O.C head-neck model developed for the current project consists of 21 835 elements. A description of elements number is summarized in Table 1.

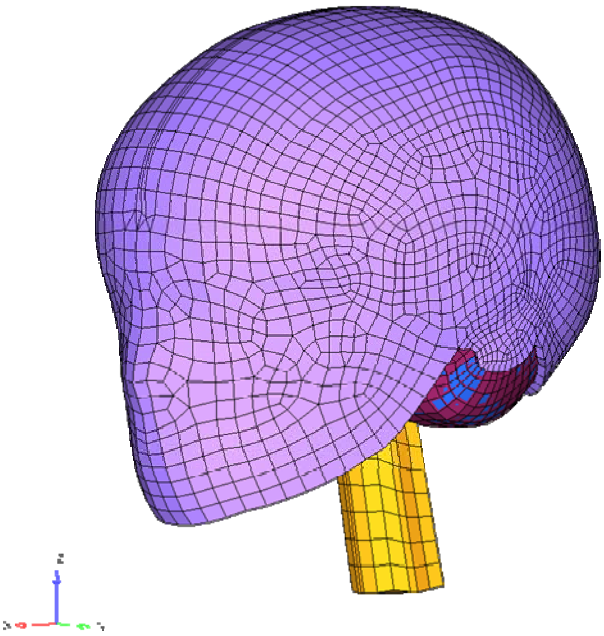

Figure 8. Overview of the 6 MOC FE head Model

	Shell	Brick
Head	4 077	17 426
Neck	164	168
TOTAL	4 241	17 594

Table 1. Number of elements used for the 6MOC head meshing

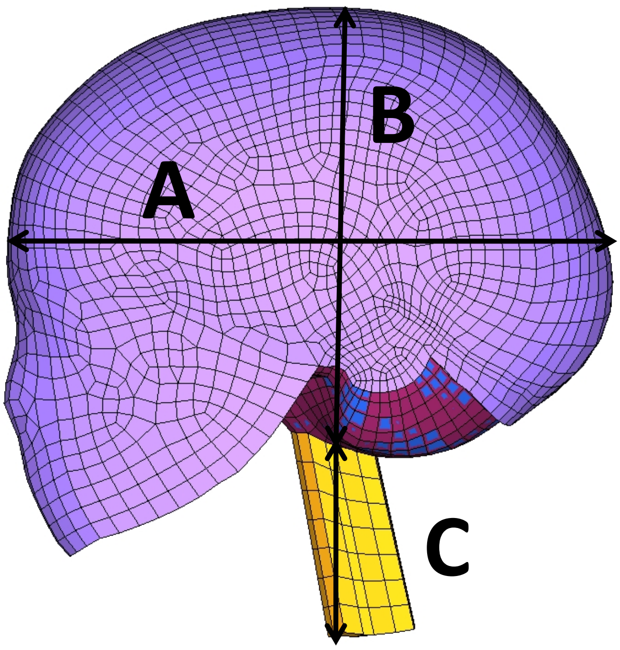

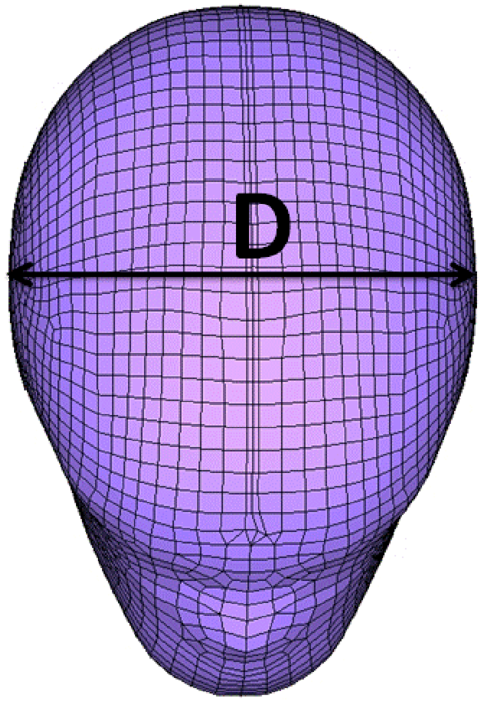

Description	**HEAD-CHILD 6 MOC (mm)**
HEAD-A	152
HEAD-B	115
HEAD-C	63
HEAD-D	112

Table 2 : Head-Neck dimension of the 6 MOC FEM

2.3 Numerical full body 6 M.O.C model (TNO contribution)

2.3.1 Method

The model was developed using the software package MADYMO, version 7.2 (MADYMO, 2010a). MADYMO is a multi-body software package that is widely used for automotive applications for fast and accurate calculations of injury risks and safety performance.

As base model for the 6-month-old baby model, the TNO's facet 50th percentile human occupant model was used and scaled down towards baby dimensions using the MADYMO/Scaler.

Since scaling from adult to children is not straightforward, a literature survey was performed to the mechanical properties (stiffness or force-displacement curves) and injury criteria for the body parts that are most vulnerable for babies in a car crash.

Next, validation data were sought in order to validate the 6-month-old baby model's responses to impact. And finally, the robustness of the model was checked by performing simulations with the baby model in a group 0 seat.

Since in CASPER Del 2.2.2 did not contain data of mechanical properties, injury criteria and validation data that could be used for a 6-month-old baby model, we performed a literature study ourselves. Due to this extra work, no time was left for validation of the baby model.

2.3.2 Scaling

As base model, the 50th percentile male occupant model as provided with MADYMO release 7.2 was used (see Figure 9). The 50th percentile male occupant model was developed and validated for impact simulation and for simulation of vibration transmission as related to seating comfort.

Figure 9. TNO 50th percentile male occupant model as released with MADYMO v7.2

The geometry of this 50th percentile male occupant model was obtained from the database of the RAMSIS software package (RAMSIS, 1997). This model consists of 92 kinematic rigid bodies. The rigid bodies form the skeleton of this human model. The human model mainly consists of chains of rigid bodies connected by kinematic joints. The first branch connects the head and vertebral bodies to the pelvis. The second and third branch connects the bodies of the left and right leg to the pelvis, respectively. The fourth and fifth branch connects the fingers to the shoulders, respectively. The thumb is connected to the mid-hand joint on a separate branch from the fingers. The thorax and the abdomen each consist of 4 flexible bodies (MADYMO Theory Manual, Koppens 1988) that divide the thorax and abdomen in horizontal slices. This construction with flexible bodies makes structural deformation of the thoracic and abdominal area possible which is important for simulations in automotive impacts.

The inertia properties of the rigid bodies and the ranges of motion of the kinematic joints were based on biomechanical data published in literature. Joint restraint, cardan restraint, point restraint, and six degree of freedom restraint models were used to model the static and dynamic joint characteristics. The joint characteristics and mechanical properties were based on biomechanical data from literature and some of them were tuned during the validation process. The human model was validated using volunteer and post mortem human subject (PMHS) responses in blunt impact tests at various locations and in full body sled tests in various directions.

The outer surface of the occupant model is described with meshes of shell-type no mass contact elements (facet surfaces). These facet surfaces are fully connected to the rigid and/or flexible bodies. Inertial properties of the occupant segments are represented fully by the inertial properties of the rigid and flexible bodies. Deformation of soft tissues (flesh and skin) is represented by stress-based contact characteristics defined for the facet surfaces. Using these contact characteristics in contact definitions, soft tissue deformation is described accurately through the contact interactions of the facet occupant model with itself and with its environment. For a more detailed description of the model please refer to the MADYMO Human Models Manual, v7.2 (MADYMO, 2010b).

The baby model's geometry was based on CANDAT geometry. CANDAT is a database containing child geometry from children of age 0 to 18 years from US, Europe and Japan (Twisk, 1994). This database was chosen, as it was also used as geometrical base for the Q-dummy family. This database makes no distinction between boys and girls. The geometric measures for the 6-month-old baby were directly available in the CANDAT database.

Using the basis human model and the geometric measures from CANDAT as input, MADYMO/Scaler created the basis of the baby model. In total 30 measures were defined from CANDAT for the scaling of the 6-month-old baby model. Since, these data from the CANDAT database are confidential, only the main geometric measures for the 6-month-old baby model that were used as input for the MADYMO/Scaler are listed in **Erreur ! Source du renvoi introuvable.**. MADYMO/Scaler keeps the standing height and the weight as fixed parameters, so input equals output. The other geometric measures of the resulting model can differ slightly from the input, since MADYMO/Scaler obeys certain scaling rules.

After the scaling various adaptations were made to the mesh to make the baby model look more like real babies based on photos of 6-month-old babies. Also, the initial position of the baby model was adapted to a typical baby position (bended arms and legs). The resulting 6-month-old baby model is shown on the lap of the TNO 50th percentile male occupant model in Figure 10.

Table 3. Main anthropometric measures for the 6-month-old child model obtained from the CANDAT database.

Geometric measure	CANDAT
weight	7.60 kg
Standing height	668 mm
Seated height	443 mm
Neck circumference	216 mm
Head length	152 mm
Head breadth	116 mm
Head to chin height	145 mm

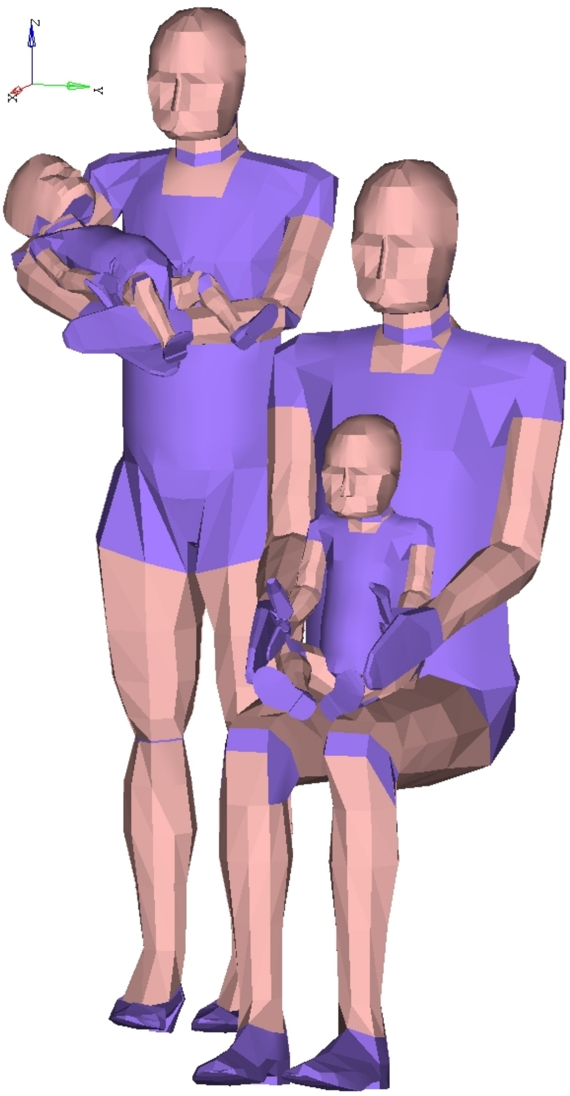

Figure 10. Resulting 6-month-old baby model on the lap of the 50th percentile male occupant model, and next to it the 5th percentile female occupant model with the 6-week-old baby model in the arms.

2.3.3 Most vulnerable body parts

CASPER Deliverable D.2.1.1 version 2 contains an accidentology study that was used here to define the most vulnerable body parts for a 6-months-old baby in a car crash. In that study it was concluded that for a 6-month-old baby rearward facing transportation is preferred, because of the neck fragility. Further, it was concluded that for a 6-month-old baby in frontal impact the head, arms and legs are most vulnerable, and secondly the abdomen and pelvis. And for side impact, it was concluded that for a 6-month-old baby the head and legs are most vulnerable, and secondly the neck, chest and arms.

Since arm, leg and pelvis injuries reported from car accidents in the CASPER accidentology study were not life threatening or caused severe disability, no special attention was given to these body parts of the baby models. However, neck, chest and abdomen injuries are not reported frequently, injuries to these body parts cause long hospitalizations, and thereby neck injuries can cause severe disability for life. Therefore, the mechanical properties and injury criteria for the head, neck, chest and abdomen were tried to find in literature in order to check and eventually update the baby model.

Literature about injury limits and mechanical properties about children is limited, and under the age of two is even more limited. This study focussed on human data, animal data were not taken into account. The literature findings about mechanical properties of babies are described below. The literature findings about injury limits that could be used for the 6-month-old baby model is summarised in **Erreur ! Référence non valide pour un signet.**. It must be noted here that the injury criteria of the Q0 dummy were the lowest values that were stated in the EEVC WG 12 report on the Q dummies.

Franklyn et al. (2007) published a review article about pediatric material properties. This study was very helpful to find data that could be used to update the 6-month-old baby model. Most of the data described below were also described in the study of Franklyn et al. (2007).

Prange et al. (2004) performed non-destructive impact tests on intact heads of newborns, 1, 3 and 11 days old, and published an elastic modulus of 50 N/mm at a 10 and 50 mm/s impact, and 7 N/mm at 0.05 mm/s. The specimens in this study were also tested in impact. The drop heights were approximately 15 and 30 cm. The orientations were chosen so that the impacts occurred in five locations: vertex, occiput, forehead, right parietal, and left parietal. So, each specimen underwent ten nondestructive drops. The peak acceleration was not significantly affected by impact location. The time history curves resulting from the drop tests showed that the shape of the curve may appear different for different conditions, but this was not statistically significant across the tests. The acceleration pulse durations were similar for the two drop heights.

McPherson and Kriewall (1980) tested the skull of two full-term neonate Post Mortem Human Subjects (PMHS) in three-point bending tests at 0.5 mm/min. In perpendicular direction they found an elastic bending modulus for the parietal and frontal bones of 0.55-1.8 GPa.

Jans et al. (1998) performed three-point bending tests on parietal bone samples from children aged 7 to 11 months at 30 mm/min. They found an elastic bending modulus of parietal bone of 1.7-3.3 GPa.

Margulies & Thibault (2000) found an elastic bending modulus for cranial bone in perpendicular direction of 820.9 MPa for a 1-week-old baby in three-point bending tests at a bending rate of 2540 mm/min. At this bending rate, rupture of the cranial bone from a 1-week-old of occurred at 10.6 MPa. And for a 6-month-old baby an elastic bending modulus of 2.11-3.58 GPa was found at bending rates of 2.45-2540 mm/min, and rupture occurred at 42.1-71.1 MPa. The elastic bending moduli that were found by Margulies & Thibault (2000) comply with the findings of McPherson and Kriewall (1980) and Jans et al. (1998).

Runge et al. (1998) tested samples containing coronal, sagittal, or metopic sutures from 3- to 15-month-old child PMHSs in tension at 30 mm/s. The sample orientation was not mentioned. In this study, it was demonstrated that the behavior of sutures, like most biological materials, was nonlinear. The stiffness of the suture was calculated from the linear portion of the curve and had a value of 189 N/mm.

Ouyang et al. (2005) found that the rotational and linear stiffness of the neck is independent of age between 2 and 12 years. Failure load was age dependent in the tested age group. The average ± standard deviation rotational stiffness of the skull–C2, C2–T2, and skull–T2 spinal segments was 0.72 ± 0.07, 0.07 ± 0.02, and 0.04 ± 0.01 Nm/degree, respectively. The average linear stiffness of the neck in tensile loading was 34.7 ± 5.7 N/mm. In the destructive tensile tests with the 2-4-year-old specimens, failure occurred at an average distraction force of 595 ± 143 N and an average distraction displacement of 20 ± 3 mm. The youngest that was tested was a healthy 2-year-old that died of poisoning. In the destructive neck tensile test, the neck failed at 500 N, due to a fracture of the superior end-plate of C6.

Luck et al. (2008) tested eighteen PMHS osteoligamentous head-neck complexes in tension ranging in age from 20 weeks gestational to 14 years. After non-destructive tests were conducted, each segment was failed in tension. The tensile stiffness of the whole spines ranged from 5.3 to 70.1 N/mm. The perinatal and neonatal specimens had an ultimate strength for the upper cervical spine of 230.9 ± 38.0 N and for the lower cervical spine of 212.8 ± 60.9 and 187.1 ± 39.4 N for the C4-C5 and C6-C7 segments, respectively. When compared to the study of Ouyang et al. (2005), it seems that the neck strength is weaker for children under the age of 2 years.

Ouyang et al. (2006) performed thoracic impact tests on four PMHSs of 2 to 4 years old impacted with a 2.5 kg mass impactor of 5 cm diameter at a nominal 6 m/s velocity. The test results demonstrated an average initial stiffness of approximately 60 N/mm. The mean values of peak sternal viscous criterion (V*C) and accelerations were 2.05 ± 0.5 m/s and 65 ± 20.1 g, respectively. The maximum forces were 776.3 ± 39 N. Several subjects sustained injuries during these impact tests.

Sandoz et al. (2011 in press) published a study about thoracic stiffness calculated from children in treatment for respiratory diseases. The patients were lying on a 9 mm thick foam mattress in supine position. A physiotherapist put one hand on the abdomen and the other on the thorax in the middle of the sternum. The physiotherapist made multiple compressions to increase the expiratory flow. These compressions were performed in synchronization with the respiratory cycle, during the exhale phase of voluntary breathing. During the treatment the force on and displacement of the thorax were measured. For a 1.5 month old baby a maximum force of 176-203 N was registered with a maximum displacement of 14 mm.

Unfortunately, no relevant data specifically about the abdomen were found for a 6-month-old baby model. Using all the stiffness values mentioned above the joint characteristics of the 6-month-old baby model were checked and updated where this was needed.

Table 4. Literature findings for injury limits of the main body parts for babies.

Body part	Load	Injury limit	Injury	Comment	Reference
Head	Three-point bending	10,6 MPa	Cranial bone rupture	1-week-old, bending rate 2540 mm/min	**Margulies & Thibault (2000)**
	Three-point bending	42,1-71,7 MPa	Skull fracture	6 month old, bending rate 2.54-2540 mm/min	**Margulies & Thibault (2000)**
	HIC_{36}	477	ECE R94 scaled	IARV Q0 dummy	**EEVC WG12 report**
	HIC_{36}	523	20% AIS3+	IARV Q0 dummy	**EEVC WG12 report**
	HIC_{36}	631	50% AIS3+	IARV Q0 dummy	**EEVC WG12 report**
	A_{3ms}	79 g	ECE R94 scaled	IARV Q0 dummy	**EEVC WG12 report**
	A_{3ms}	85 g	20% AIS3+	IARV Q0 dummy	**EEVC WG12 report**
	A_{3ms}	97 g	50% AIS3+	IARV Q0 dummy	**EEVC WG12 report**
Neck	Tension	725 N	Decapitation	2-week-old	**Duncan, 1874**
	Tension	654 N	Spinal column failure	2-week-old	**Duncan, 1874**
	Tension	500 N	Fracture of superior end-plate at C6	Healthy 2-year-old	**Ouyang et al. (2005)**
	Tension	200 N	Spinal column failure	Perinatal and neonatal	**Luck et al. (2008)**
	Tension	433 N	ECE R94 scaled	IARV Q0 dummy	**EEVC WG12 report**
	Tension	498 N	20% AIS3+	IARV Q0 dummy	**EEVC WG12 report**
	Tension	546 N	50% AIS3+	IARV Q0 dummy	**EEVC WG12 report**
	Flexion	13 Nm	ECE R94 scaled	IARV Q0 dummy	**EEVC WG12 report**
	Flexion	17 Nm	20% AIS3+	IARV Q0 dummy	**EEVC WG12 report**
	Flexion	20 Nm	50% AIS3+	IARV Q0 dummy	**EEVC WG12 report**
Thorax	Static compression force	176-203 N		1.5 month	**Sandoz et al., 2011**
	Static displacement	14 mm		1.5 month	**Sandoz et al., 2011**
	Dynamic compression force	776 N ± 39N		2-4 year old, 2,5 kg impactor, 5 cm diameter, at 6 m/s	**Ouyang et al., 2006**
	Dynamic displacement	48.1 ± 6.4 mm		2-4 year old, 2,5 kg impactor, 5 cm diameter, at 6 m/s	**Ouyang et al., 2006**

2.3.4 Validation

Validation of the baby model could be done by simulating an impact or deformation test performed with a child PMHS or volunteer of approximately the same age, and comparing the calculated responses with the measured responses in the test.

The study of Prange et al. (2004), as described in Section 2.3.3, could be used to validate the baby model's head in a low severe impact situation. The response of the baby model's head can be validated by comparing the time history curves of the head acceleration as measured during the non-destructive head drop tests by Prange et al. (2004) to that of the baby model in a simulation of such a drop test. When using this data for validation of the 6-month-old baby model, it must be taken into account that the head mass and the stiffness of a 6-month-old baby will be higher than that of a new born.

For the thorax of the baby model several studies could be used for validation of the thorax response to impact. However, all three studies have their limitations for validation of a 6-month-old baby model.

Kallieris et al. (1976) performed a sled impact test with a 2.5-year-old PMHS in a booster seat subjected to a deceleration of 30.7 m/s with an average acceleration of 18 G and approximately 60 ms duration. The response of the thorax-abdomen area of the baby model could be validated by comparing the measured belt loads to the belt loads resulting from a simulation of this test. And, the measured head trajectories could be used to validate the head-neck kinematics of the baby model in such a simulation. When using these data for validation of the 6-month-old baby model, it should be taken into account that a 6-month-old baby has a weaker neck and a more compliant thorax than a 2.5 year old child. Other limitations of this study are that the information on the booster seat and the belts are poorly described in this publication. The main focus on this paper was comparison between crash test dummy and PMHS responses rather than creation of validation data.

The study of Ouyang et al. (2006), as described in Section 2.3.3, could be used to validate the thorax response of the baby model for high severe frontal impact. From this study the thorax force-deformation characteristics, peak sternal viscous criterion (V*C), and T4 acceleration of the 2-4-year old cohort could be used to validate the thorax response of the baby model resulting from a simulation of this test. Also, here it should be taken into account that a limitation of this study is that the thorax of a 6-month-old is more compliant than that of a 2-4-year old.

The study of Sandoz et al. (2011 in press), as described in Section 2.3.3, could be used to validate the thorax response of the baby model for low severe loading. The thorax force-displacement curves and the thorax viscous criterion (V*C) measured and calculated from eight patients of 5 to 7 months old could be used to validate the 6-week-old baby model's thorax response resulting from a simulation of the treatment. A limitation of this study is that the compressions made on the table without a patient showed a maximum target displacement of 2.3 mm for a corresponding loading of 150 N. This displacement was attributed to the compression of the soft tissues of the hands, the compression of the mattress and the deformation of the table. This global displacement of the system was then considered to be a part of the measurement error, and was not used to determine the trunk displacement. Consequently, the displacement results were slightly overestimated.

This study was limited to the creation of a 6-month-old baby model. The validation of this model will be performed in future internal or external projects.

2.3.5 Verification

Two simulations were performed to test the robustness of the baby models. The 6-month-old baby model was positioned in a multi-body (facet) model of a group 0 seat. Next, a deceleration (frontal impact of the car), with a triangular shape with a peak of 27 G and duration of 150 ms, was applied to the seat which was in rearward position fixed with belts to a rear car seat. This resulted in rearward loading of the baby model. The simulation was repeated with the same pulse applied as an acceleration (rear end impact of the car), resulting in frontal loading of the baby model. Figure 116 shows the 6-month-old baby model in these simulations.

The resulting kinematics of the 6-month-old baby model in the robustness simulations are shown in Figure 127. The authors of this study think that the baby model showed robust and realistic behaviour in both simulations.

Figure 11. 6-month-old baby model in a rearward facing child seat.

T=50ms

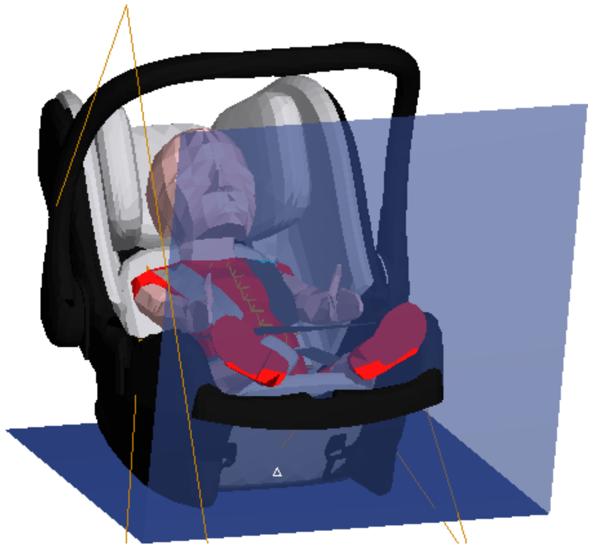

T=50

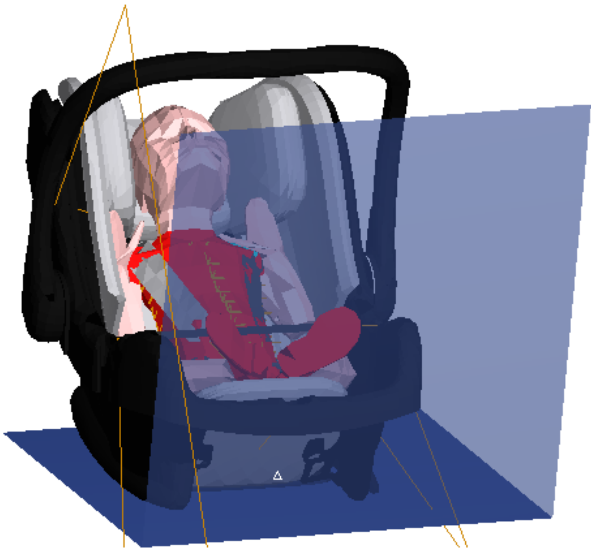

T=100ms

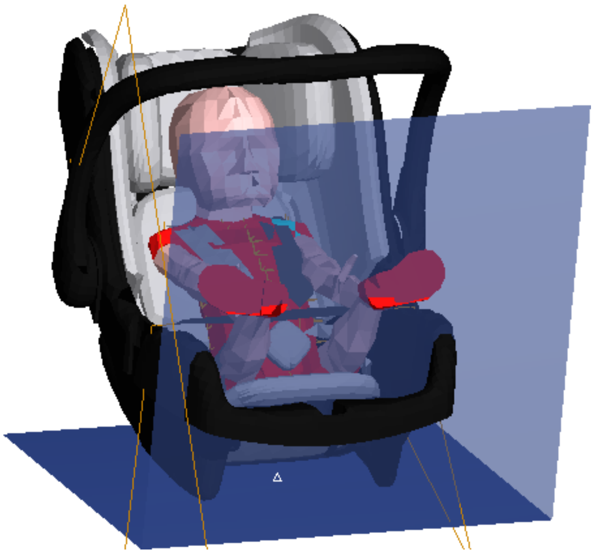

T=100

T=150ms

T=150

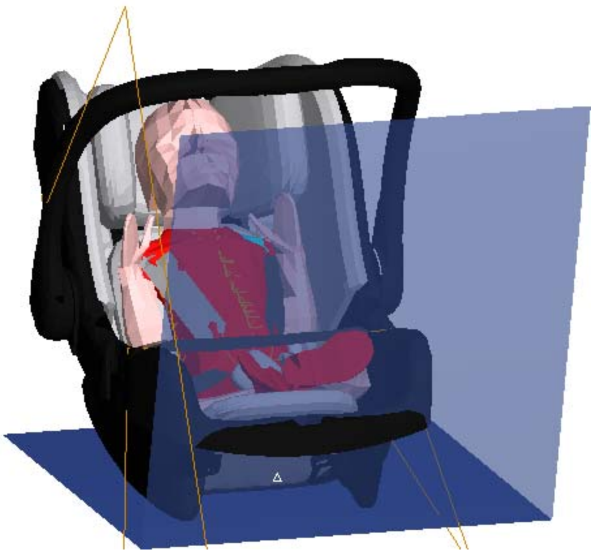

T=200ms

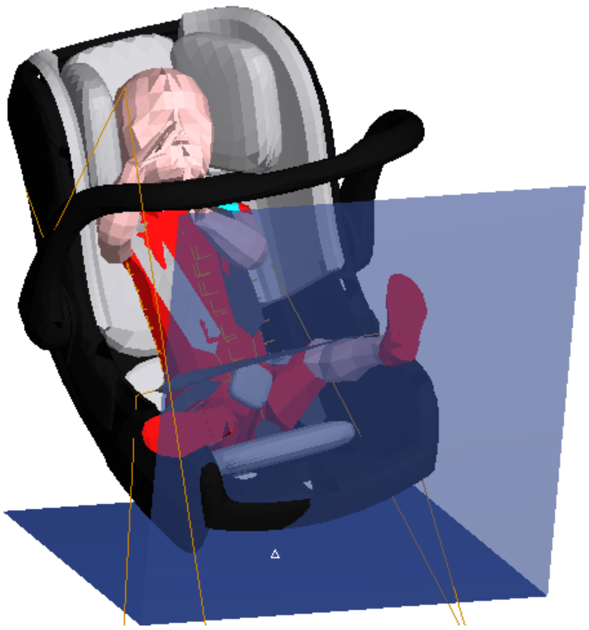

T=200

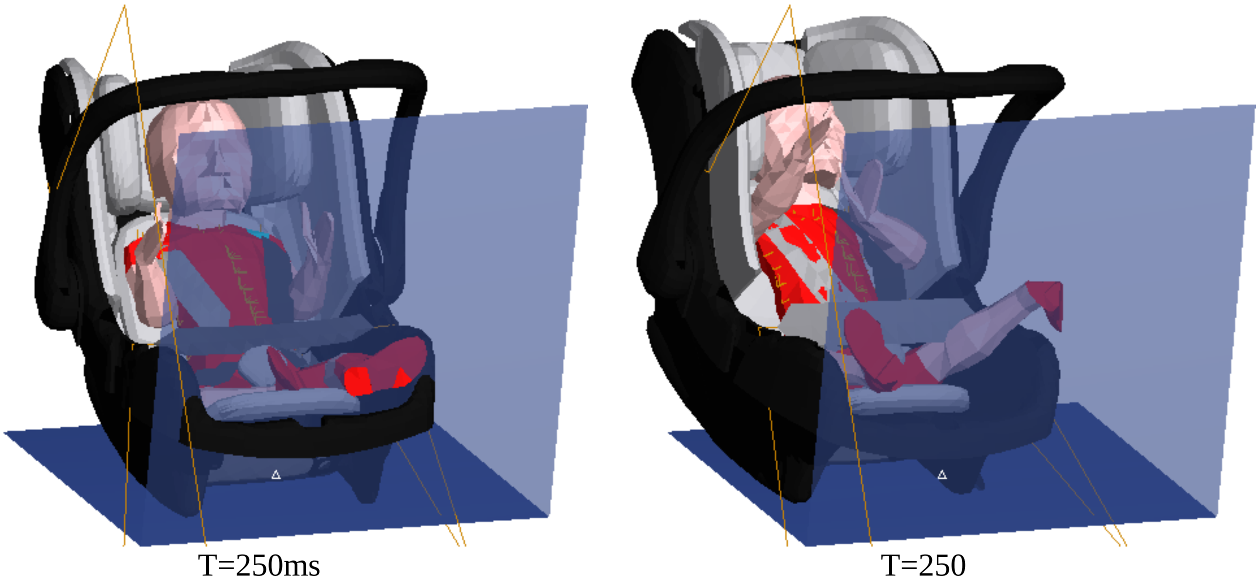

Figure 12. Robustness simulations of the 6-month-old baby model in a group 0 seat fixed to a rear car seat by belts. Left: subjected to a deceleration pulse (frontal car crash). Right: subjected to an acceleration pulse (rear end car crash).

2.3.6 Conclusions

The objective of this study was to create a multi-body 6-month-old baby model. From this study it was concluded that we successfully created a robust and calculation time efficient baby model. Mechanical properties and injury limits of the head, neck and thorax of babies between 5 and 7 months old are available. However, validation data of babies of this age are very limited. Scaling of validation tests of other age children would be needed to extensively validate this baby model.

3 1 Y.O.C. FE Model

3.1 Introduction

The starting point of the 1 Y.O.C. model is the DICOM data provided by LMU. The data comes from an 11months 21 days old child with a height of 78cm and weight of 9.6kg. The cause of death was an infection. In this section, UdS contribution for the head-neck modeling and CHALMERS contribution for the rest are presented.

3.2 The 1 Y.O.C. HEAD Model (UdS contribution)

3.2.1 Introduction

The report D2.1.1 (Report on relevant children injury in road accident and specification of children segment models as a function of age) proposed injury priorities by age and segments. Based on this report, it was decided to focus on skull fractures and head injuries. A deformable approach will be used and the following choices were made:

- The mesh was continuous between the different anatomical structures to optimize time step by reducing interfaces in the whole 1 Y.O.C. model
- A special attention was paid on mesh quality for time step reason
- Hexa elements and quads were used for all parts of the head

In this section, all anatomical features of the 1 Y.O.C. head model is presented. Element numbers and quality are reported for each segment (membranes, brain, CSF, skull, face and scalp).

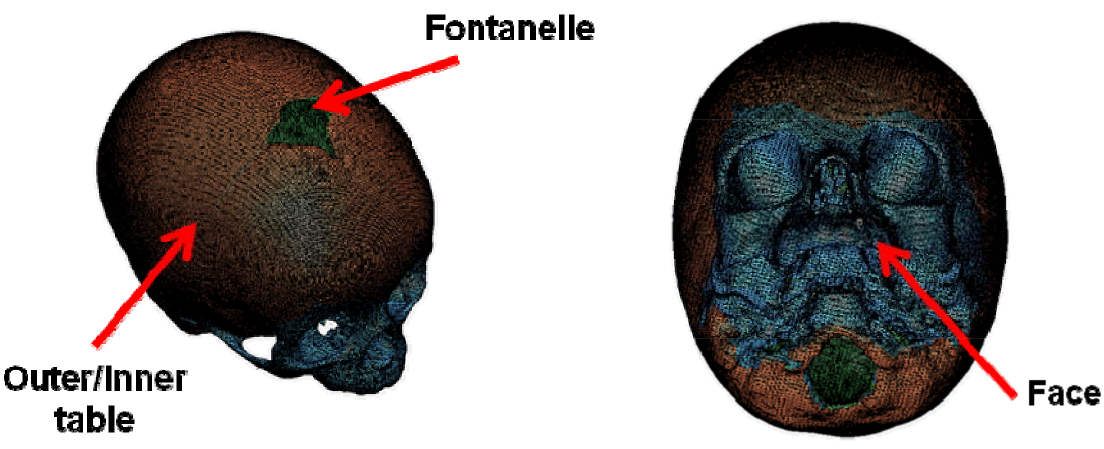

Figure 13. Overview of the segmentation of the 1 Y.O.C. external/internal skull and mandibular bones

3.2.2 Meshing of the membranes

The Falx is a thin arched fold of dura mater which descends vertically in the longitudinal fissure between the cerebral hemispheres.

The tentorium is an extension of the dura mater that separates the brain and the cerebellum. The tentorium is an arched lamina, elevated in the middle and inclining downward toward the circumference. It covers the superior surface of the cerebellum and supports the occipital lobes of the brain.

Geometries of these two membranes were defined by using some anatomical atlas and internal skull geometry provided by LMU in order to define tentorium angle. Tentorium is attached, behind, by its convex border, to the transverse ridges upon the inner surface of the occipital bone encloses the transverse sinuses. It was the first step of head meshing an illustration of the positioning of these two membranes is given in Figure 1413.

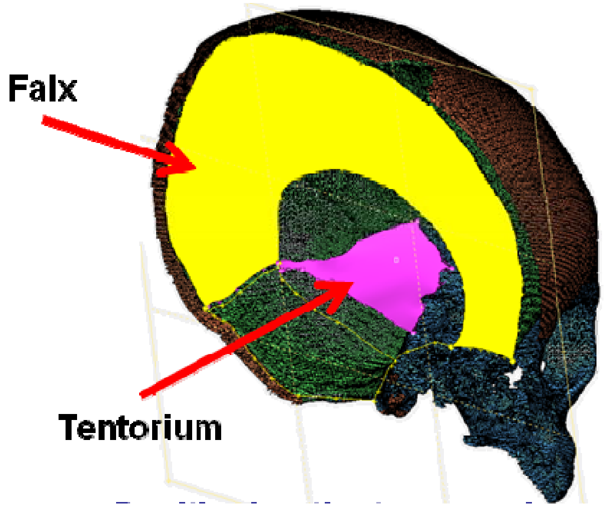

Figure 14. Positioning of the two membranes (falx and tentorium)

These thin membranes have been meshed with shell elements with four nodes (quad elements). An illustration of the meshing of these membranes is proposed in Figure 1514. Element numbers and quality as computed by the Hypermesh 10 software package (Altair Engineering) are summarized in Figure 1514.

Finally, the falx and tentorium are meshed with 323 and 440 deformable shell elements respectively.

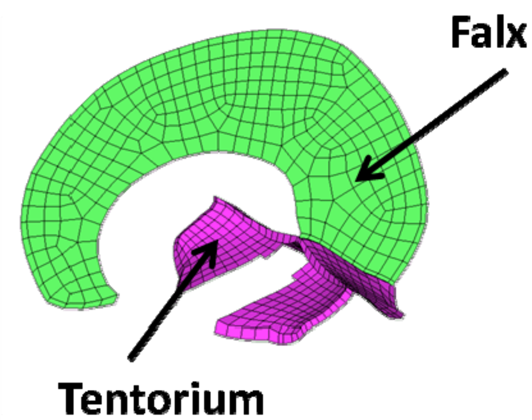

	FALX	TENTORIUM
Type of elements	Shell (quad)	Shell (quad)
Nb of elements	323	440
Max. warpage	0.0028	30.21
Max aspect ratio	4.29	4.47
Min length (mm)	1.36	0.91
Min jacobian	0.52	0.53
Min angle (°)	52.66	28.35
Max angle (°)	139.96	156.84

Figure 15. Overview of brain membranes (falx and tentorium) and mesh characteristics

3.2.3 Meshing of the brain

A special attention was given to the brain and cerebellum meshes to avoid very small elements and elements with very small or big angles that could lead to zero or negative volumes during simulations and unacceptable time steps. It was decided to use hexahedral elements.

The mesh was obtained by solid mapping. For this, two solids elements were created, one for the cerebellum and the second for the brain.

Element numbers and quality as computed by the Hypermesh V10.0 software package (Altair Engineering) are summarized in Figure 1615.

Finally, the brain and cerebellum are meshed with 10 708 brick elements; an overview of this segment is reported in Figure 1615.

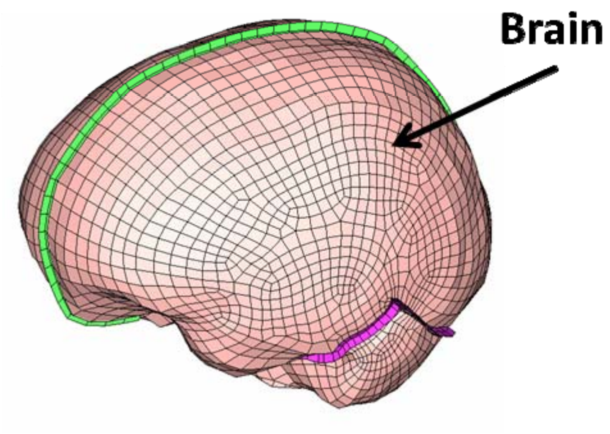

	BRAIN
Type of elements	Solid
Nb of elements	10 708
Max aspect ratio	8.78
Min length (mm)	0.68
Min jacobian	0.18
Min angle (°)	38.85
Max angle (°)	92.03

Figure 16. Overview of brain and mesh characteristics

3.2.4 Meshing of the CSF

Cerebrospinal fluid (CSF) is a bodily fluid that occupies the subarachnoid space around and inside the brain and spinal cord.

The subarachnoid space was modeled between the brain and the skull to simulate the CSF. This space is constituted by a layer of brick elements and it entirely surrounds the brain and membranes (falx and tentorium). For this, a continuous meshing between membranes and brain was applied in order to define CSF. It's an important point to reduce time step which could be appeared by creating interfaces.

Element numbers and quality are summarized in Figure 1716.

The CSF is meshed with 4116 brick elements.

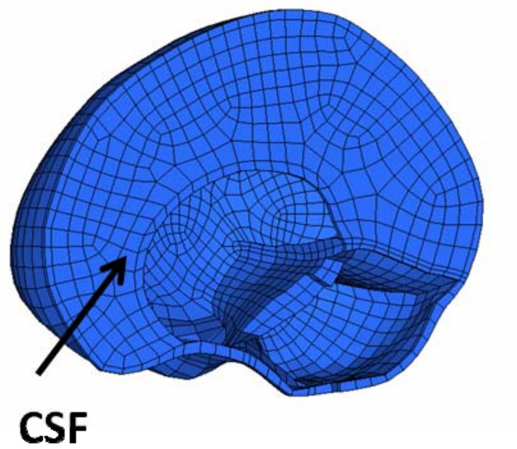

	CSF
Type of elements	Solid
Nb of elements	4116
Max aspect ratio	7.6
Min length (mm)	0.9
Min jacobian	0.24
Min angle (°)	38.85
Max angle (°)	92.03

Figure 17. Overview of CSF and mesh characteristics

3.2.5 Meshing of the Skull and face

The skull is modeled by one layer of shell elements representing the cranial bone constituted by only cortical bone for a 1 Y.O.C. A special attention will be paid on mechanical properties of this skull in order to be able to reproduce skull failure which is one of the injury mechanisms at this age.

A simple face was meshed with shell elements and will be considered as rigid during simulation. This hypothesis is justified by the fact that few face injuries are referenced in the literature for a 1 Y.O.C. This face declared as rigid body will permit to take into account its inertia and mass in the model.

Finally, the skull (including sutures) and the face are meshed with 2816 and 544 deformable shell elements respectively, an overview of these segments are reported in Figure 1817.

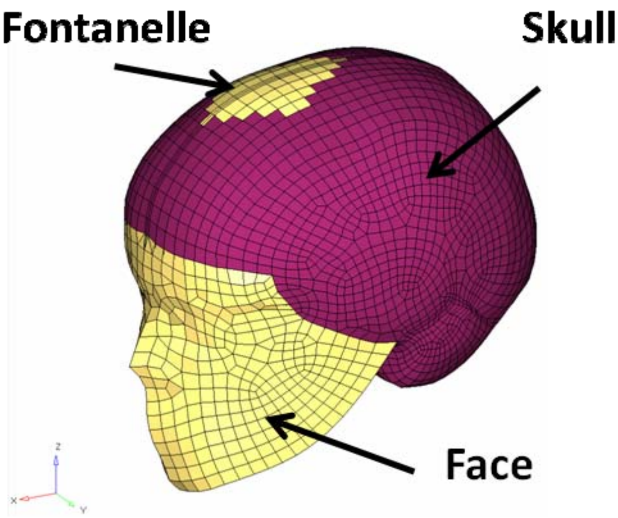

	SKULL+SUTURES	FACE
Type of elements	Shell	Shell
Nb of elements	2816	544
Max. warpage	32.63	39.1
Max aspect ratio	10.96	4.12
Min length (mm)	0..48	1.5
Min jacobian	0.45	0.48
Min angle (°)	22.86	47.52
Max angle (°)	160.41	139.64

Figure 18. Overview of bones (skull, suteures and face) and mesh characteristics

3.2.6 Meshing of the scalp

The scalp plays an important role because it's the first padding during a direct impact.
The scalp was modeled by a layer of brick elements and surrounds the skull and facial bones. An overview of scalp and mesh characteristics are given in Figure 1918. The scalp is meshed with 2744 brick elements.

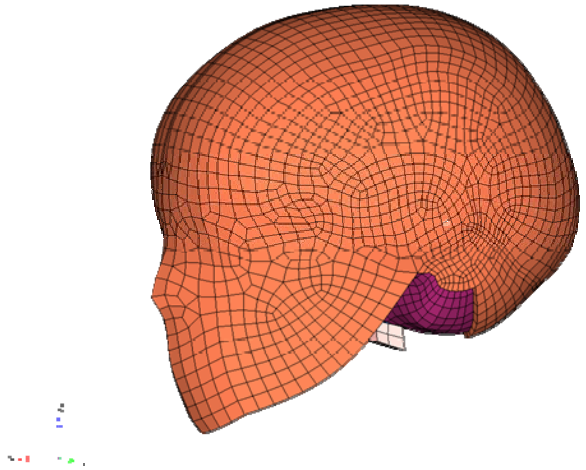

	SCALP
Type of elements	Solid
Nb of elements	2744
Max aspect ratio	7.3
Min length (mm)	0.92
Min jacobian	0.35
Min angle (°)	21.66
Max angle (°)	155.36

Figure 19. Overview of scalp and mesh characteristics

3.2.7 Conclusion

The proposed finite element head model of a 1Y.O.C. head was based on the geometrical 3D reconstruction of 2D slices obtained by CT X-Ray scanner coming from LMU.
3D triangular mesh was then generated in STL format and imported in Hypermesh V10.0, allowing regular meshing of the whole head required by explicit codes like Ls-Dyna.

The new finite element head model simulates closely the main anatomical features: skull, falx, tentorium, subarachnoid space, scalp, cerebrum, cerebellum and brainstem.
Figure 2019 illustrates the different parts of the developed model.

The finite element mesh is continuous and represents a 1 Y.O.C. head model. Globally, the 1 Y.O.C head model developed for the current project consists of 21 707 elements. A description of elements number by part is given in Table 5.

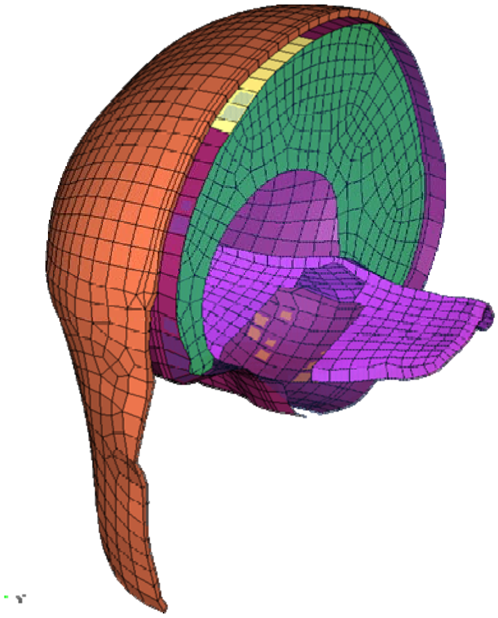

Figure 20. Overview of the 1 Y.O.C. FE head Model

	Shell	Brick
Falx	323	
Tentorium	440	
Brain		10 724
CSF		4 116
Skull+suture	2 816	
Face	544	
Scalp		2 744
TOTAL	4 123	17 584

Table 5. Number of elements used for the 1 Y.O.C. head meshing

3.3 The 1 Y.O.C. NECK FE model (UdS contribution)

Based on a Scanner of a 1 YOC provide by LMU this file was then imported under Hypermesh (cf Figure 2120). The surfaces of each of the cervical vertebrae were reconstructed, than the cervical vertebrae could be completely meshed.

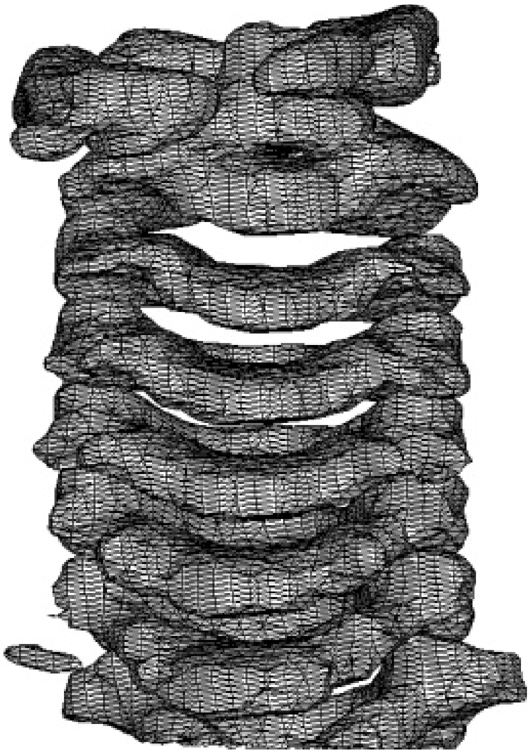

Criterion	Values
Length min.	1 mm
Length max.	1.5 mm
aspect ratio	[1-2]
warpage	[0-5]
angle quad (°)	[70-110]
angle tria (°)	[50-80]
Jacobien	[0.7-1]
% of trias	6

Figure 21: Reconstruction of the cervical spine based on scanner sections

Table 6 : Meshing criteria allowing the calculation time to be optimised.

The cervical vertebrae were modelled using shell elements (Figure 2221 - Figure 2423), the intervertebral discs with brick elements (Figure 2524) and the ligaments with spring elements.

The modelling option for vertebra is justified as shell elements offer the possibility to strictly respect the anatomical surface and to declare this part as a rigid body in order to respect the geometry of the articular surfaces and to correctly reproduce the inertias.

The option to represent the intervertebral discs with bricks elements (5 layers) is justified by the need to reproduce the 3D shearing behaviour of this structure.

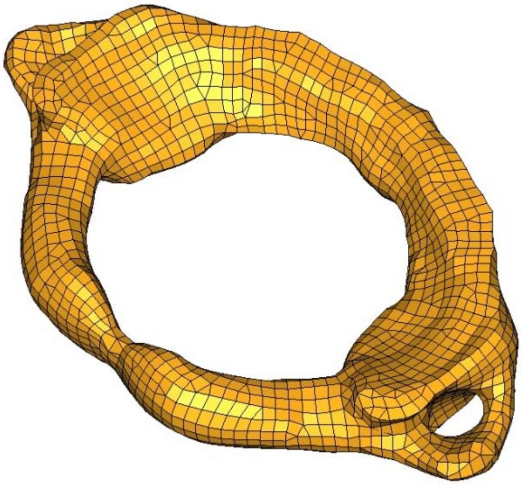

Figure 22 : Atlas (Shell elements)

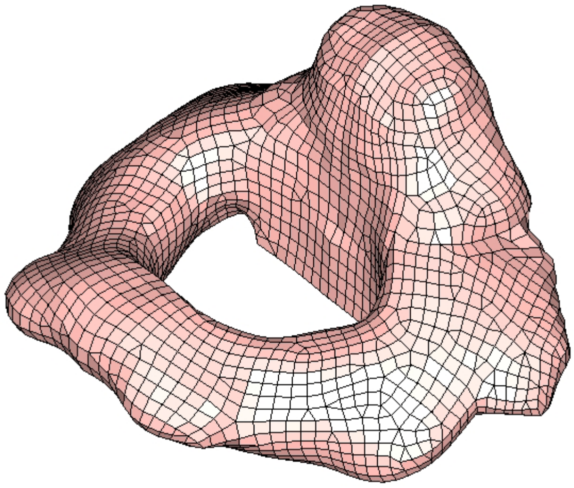

Figure 23 : Axis (Shell elements)

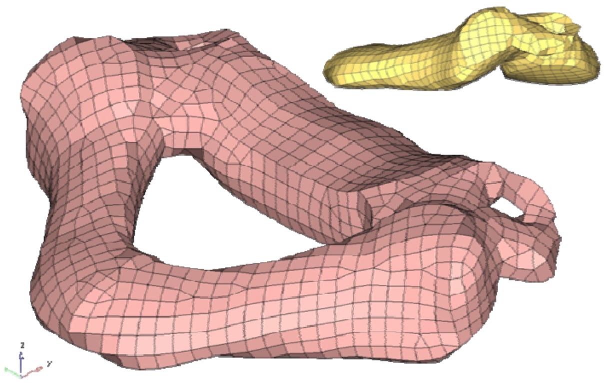

Figure 24: C3 (Shell elements)

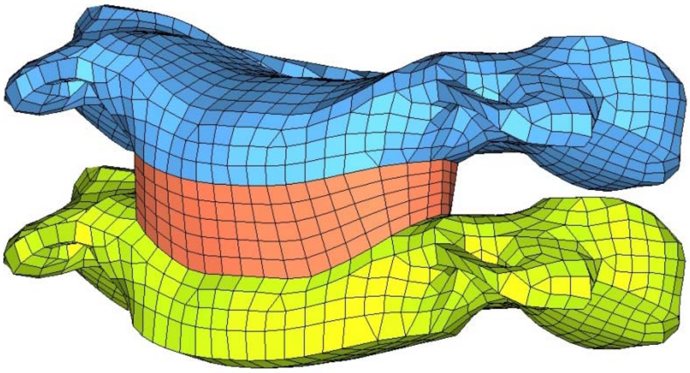

Figure 25 : Intervertebral disc (Solid elements)

As far as the lower cervical spine is concerned, five types of ligaments were distinguished as shown in Figure 2625. The anterior longitudinal ligament (ALL), the posterior longitudinal ligament (PLL), the flavum ligament (FL), the interspinal ligament (ISL) and finally the capsular ligaments (CL) (Figure 2625).

For the upper cervical spine, the posterior common ligament (C2-C0; C2-C1; C1-C0), the atloidien-axoidien anterior ligament, the transverse ligament, the yellow ligament (C2-C1), the transverse axoid ligament, the anterior occipito-atloid ligament, the alar ligament, the posterior occipito-atloidien ligament, the capsular ligament C2-C1, the capsular ligament Head-C1, membrane tectaria, the median occipito-odontoid ligament as well as the lateral occipito-atloidien ligament were modelled as illustrated in Figure 2726.

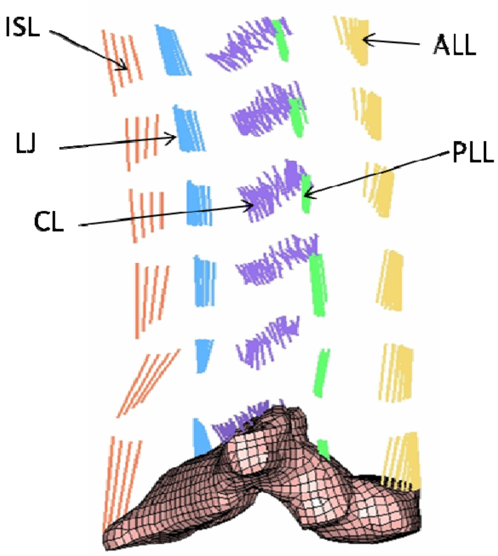

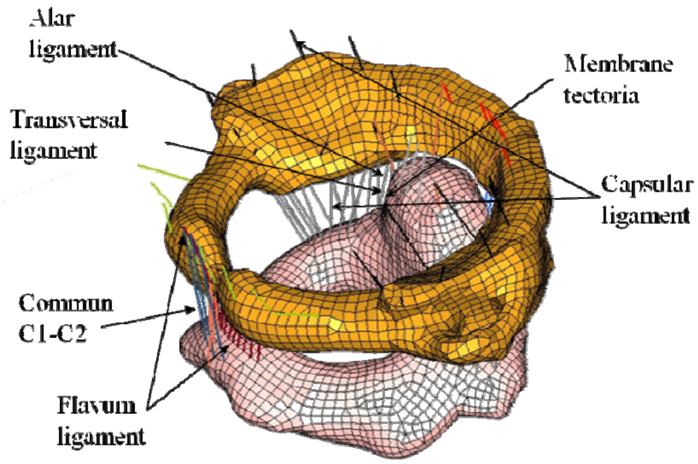

Figure 26 : Ligamentary system of the lower spine (with The anterior longitudinal ligament (ALL), the posterior longitudinal ligament (PLL), the flavum ligament (FL), the interspinal ligament (ISL) and finally the capsular ligaments (CL).

Figure 27 : Ligamentary system of the upper spine (with posterior common ligament (C2-C0; C2-C1; C1-C0), the atloidien-axoidien anterior ligament, the transverse ligament, the yellow ligament (C2-C1), the transverse axoid ligament, the anterior occipito-atloid ligament, the alar ligament, the posterior occipito-atloidien ligament, the capsular ligament C2-C1, the capsular ligament Head-C1, membrane tectaria, the median occipito-odontoid ligament and the lateral occipito-atloidien

As a whole, the finite element model of the neck system thus defined consists of elements divided into 17 496 shell elements, 555 spring elements and 3720 volume elements. A more global representation of the model is given in Figure 2827.

Figure 28 : Global overview of the cervical spine

3.4 Head and Neck coupling of the 3YOC model (UdS contribution)

The connection between the head and the neck is done by the ligamentary system. The ligaments involved are: the commun ligament, the occipito-transverse ligament, the capsular ligaments, the flavum ligament, the membrane tectoria, the alaire ligament and the occipito-atloidien lateral ligament. A sliding interface is implemented in order to simulate the local behavior of the facet joint between the atlas and the head. A global overview of the head-neck system are illustrated in the Figure 2928

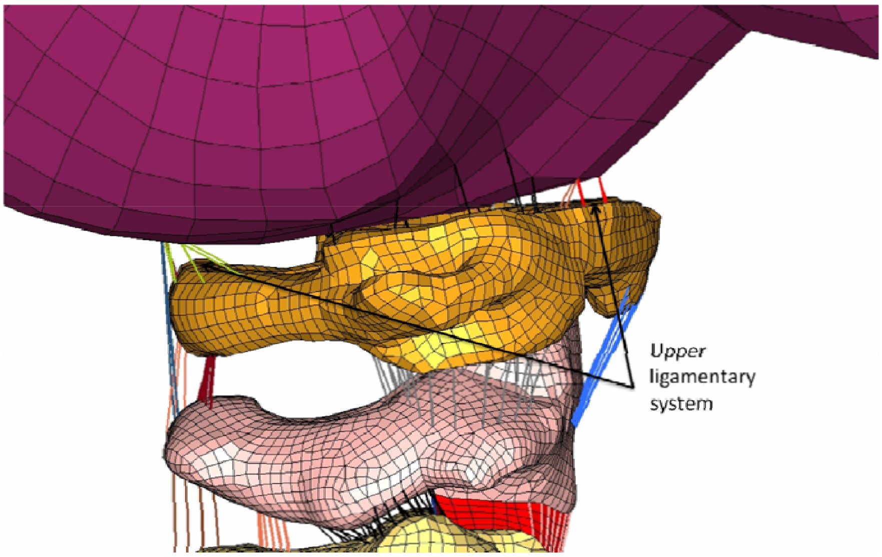

Figure 29. Zoom on the atlanto-occipito joint and the ligamentary system.

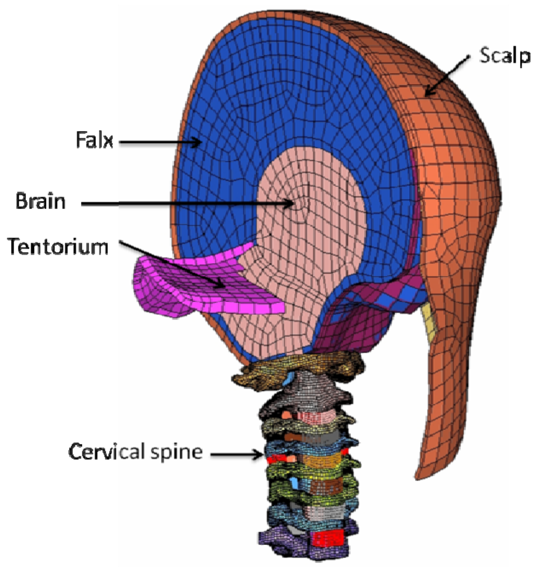

Figure 30 : Section of the 3 YOC Head-Neck system

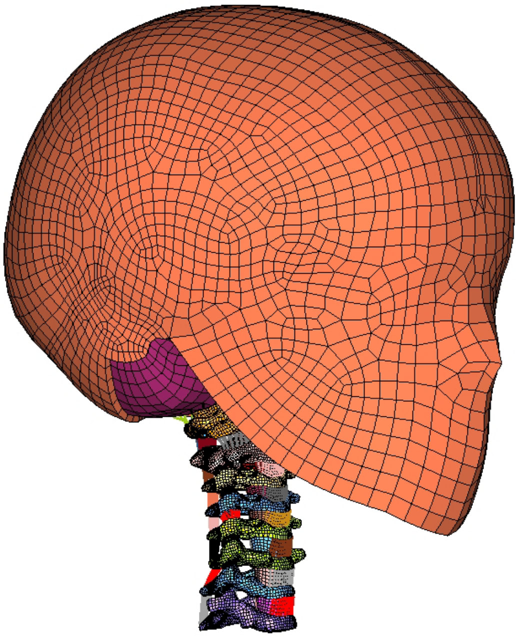

Figure 31 : Global overview of the 1 YOC Head-Neck system.

Head-Neck dimension are summarize in Table 7.

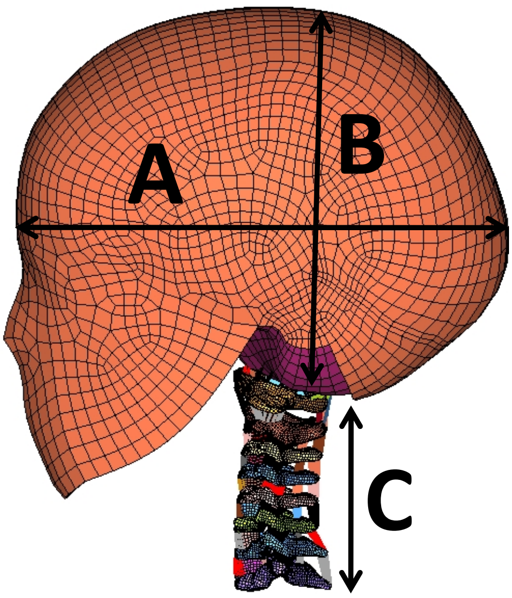

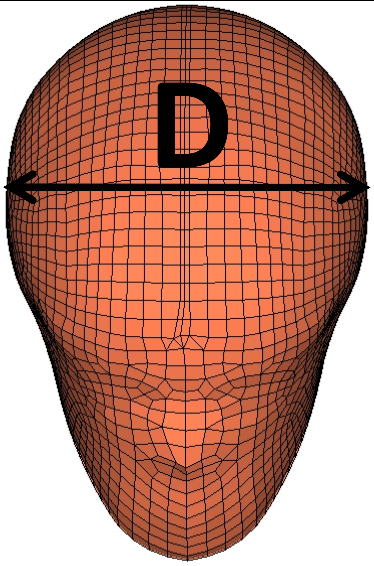

Description	HEAD-CHILD 1 YOC (mm)
HEAD-A	160
HEAD-B	123
HEAD-C	70
HEAD-D	120

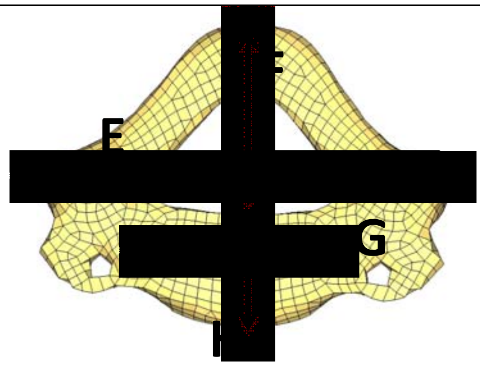

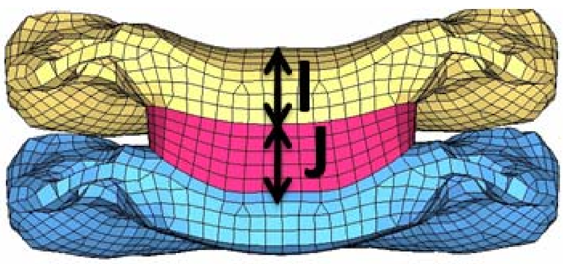

Description	CERVICAL-CHILD 1 YOC (mm)
T1-C7-K	5
C7-E	35
C7-F	21
C7-G	15
C7-H	9.5
C7-I	3.6
C7—C6-J	4.6
C6-E	34
C6-F	18
C6-G	16
C6-H	7.7
C6-I	4
C6—C5-J	5.4

C5-E	33
C5-F	17
C5-G	17
C5-H	8
C5-I	4
C6-C5-J	5
C4-E	32
C4-F	17
C4-G	17
C4-H	8
C4-I	3.5
C4—C3-J	4.5
C3-E	33
C3-F	17
C3-G	17
C3-H	8
C3-I	3.5
C3—C2-J	4.5
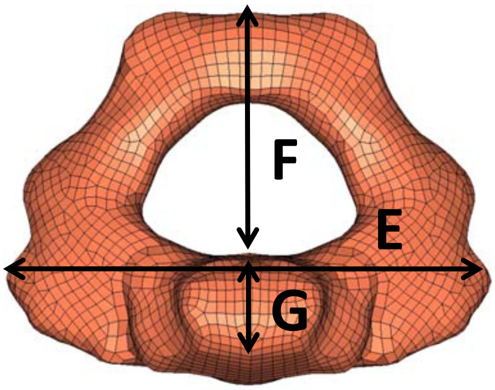	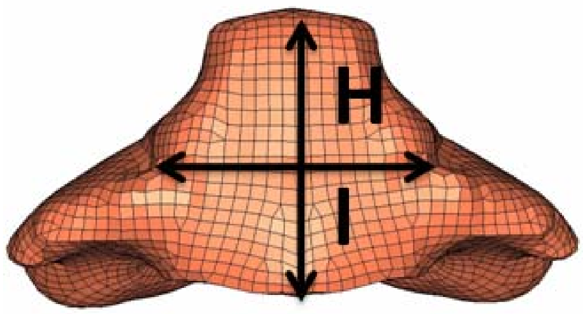
C2-E	38
C2-F	18
C2-G	7
C2-H	15.5
C2-I	17.5
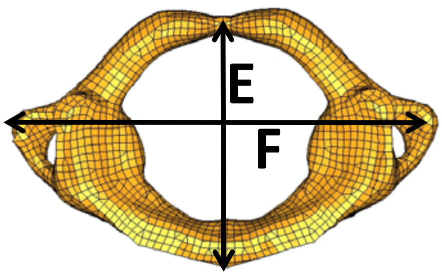	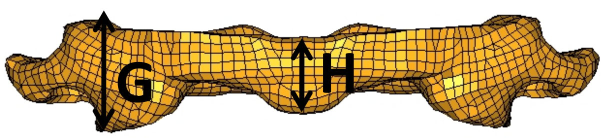
C1-E	52
C1-F	31
C1-G	9
C1-H	7

Table 7: Head-Neck dimension of the 1 YOC FEM

3.5 1 Y.O.C. FE Thorax, Abdominal and lower legs model (CHALMERS contribution)

3.5.1 Introduction

Chalmers contributed to subtask 2.3.2 with the aim at development of an FE model of 1 year old child. The initial geometry information on the whole skeleton of the child is presented in STL files "skeleton.stl". The geometry information on the whole skin of the child is presented in another STL file "skin-1YOC.stl". This subtask will develop the mesh layout of the whole body of the child FE model. Including the whole skeleton and the ligaments and flesh attached to them. The mesh layout of the head and neck will be developed by UDS.

3.5.2 Meshing of the skeleton

Figure 3231a demonstrated the original geometry the skeleton in the STL file "skeleton.stl" which was imported into HyperMesh platform. In this model, the skeleton of the whole child body is presented as one part and constructed by triangle shell elements.

3.5.2.1 Strategy of remeshing the skeleton

As shown in Figure 3231 b the skeleton of each anatomy parts were separated from the whole body and demonstrated by the different colors. In the first step, the skeleton was divided into tow parts along with the sagittal plan. All the bones of the right side were re-meshed by using solid elements and reflected to the left side of the skeleton to form the complete skeleton of the whole body except for skull and cervical spine. The locations of the reflected bones were adjusted so as to coincide with the initial bones of the left side.

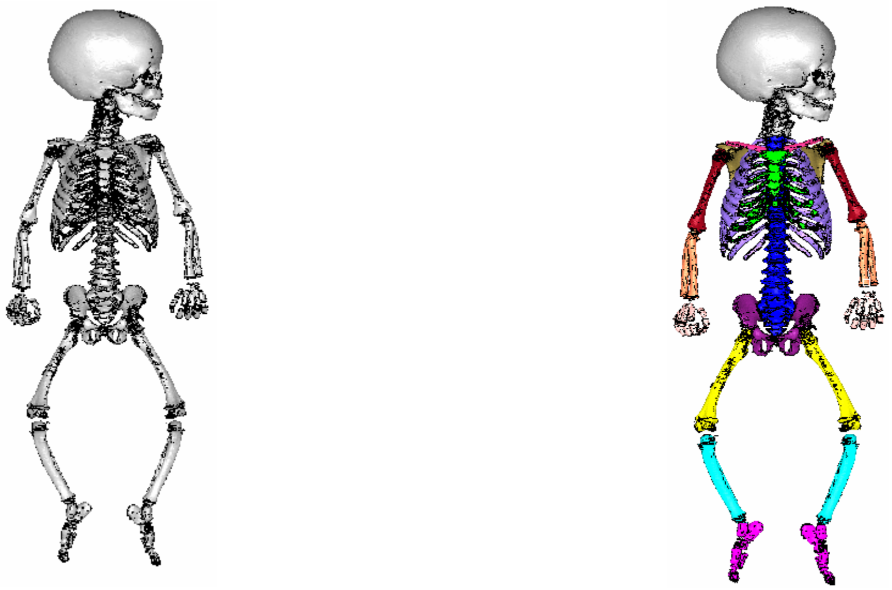

(a) Initial geometry model (b) Models of each anatomy segment

Figure 32 : Skeleton of whole child body

3.5.2.2 Cleanup of initial geometry

The geometry of the initial skeleton was not ready for the remeshment of the model. The problems include unreasonable deep concaves, prominent convexes, unreasonable connection between bones, and doubled layers of bones. Therefore, the initial geometry of the bones must be cleaned up and smoothed. Those problems can be solved by deleting the original elements, creating smooth surfaces covering empty areas, and auto-meshing smooth surfaces.

3.5.2.3 Meshing of the long bones

When the geometry of a long bone (humerus , ulna , radius , clavicle , femur, tibia , fibula) was cleaned up, the surface of the long bone was created. Based on the surface of the long bone, the solid was created as shown in Figure 3332a. Then the long bone was cut to six parts by using these cutting lines (Figure 3332b) . As shown in Figure 3332c, three different types of parts were separated from the long bone. Part 1 is regular shaft, and each piece of the shaft can be re-meshed by solid elements. Part 2 and part 3 are misshapen, and must keep the character of the joint surface. So the elements of those two parts should be meshed precisely. The whole long bone was re-meshed as shown in Figure 3332f.

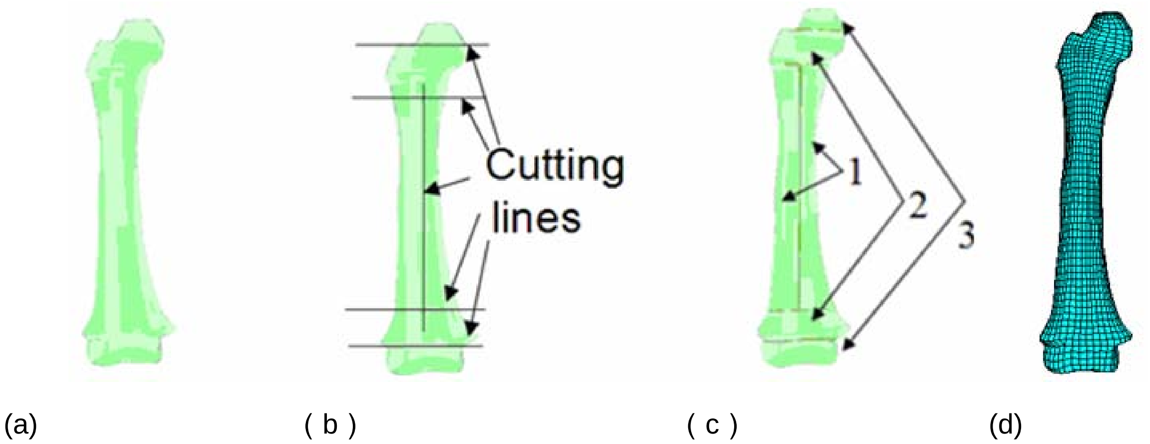

Figure 33 : Meshing of right femur

By using the same method, other long bones of the right side were re-meshed by solid elements, then duplicated and reflected these elements to the left side. It was relocated according to the positions of the initial left long bones. All long bones were re-meshed as shown in Figure 3433.

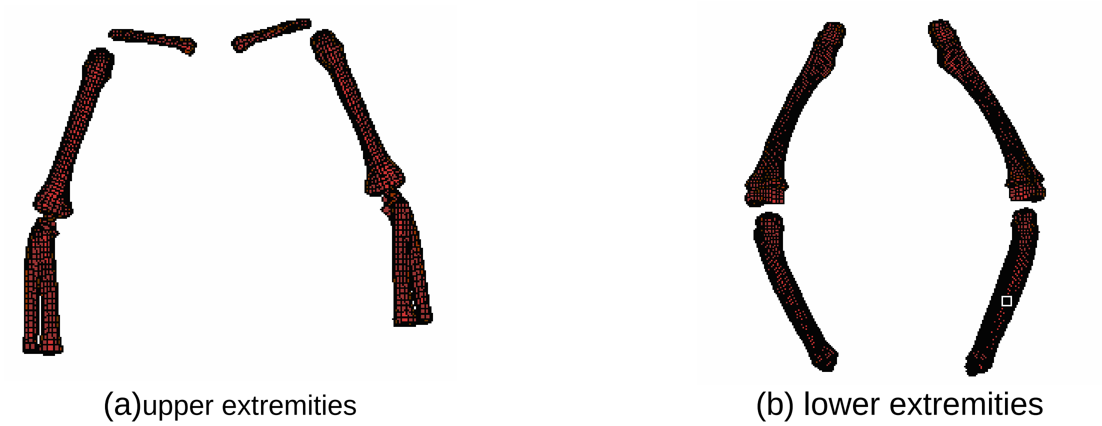

Figure 34 : Meshing of the long bones

3.5.2.4 Meshing of the vertebras

The vertebras are more misshapen than the long bones. The interface between vertebra and disc should be smoothed and connected by sharing nodes. So it is important to clean up and split the initial geometry for creating of new mesh layout of the vertebras. As shown in Figure 3534a, each vertebra was separated into four parts. Part 1 is vertebra body, on the end surface should share notes with the disc. Part 2 is pedicle of vertebra arch. Part 3 is spinous process. Part 4 is transverse process. The four parts should be meshed one by one. As shown in Figure 3534b part 1 was meshed by using solid element. As shown in Figure 3534c, the shell elements covering the interface of part 1 and part 2 were created. Based on the shell elements, the upper part of part 2 could be meshed, as shown in Figure 3534d. By the same method, other parts of the vertebra can be meshed (Figure 3534e).

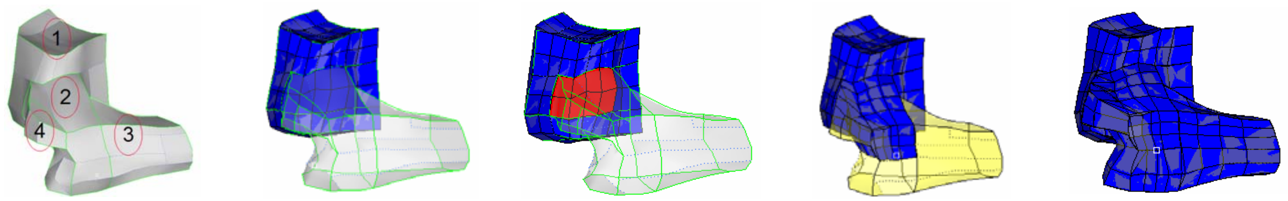

(a) (b) (c) (d) (e)

Figure 35 : Meshing of the vertebra

Using the same method, other vertebras of the lift side were remeshed by solid elements, then duplicated and reflected these elements and relocated the reflected elements according to the positions of the initial geometry. All vertebras and discs were remeshed as shown in Figure 3635.

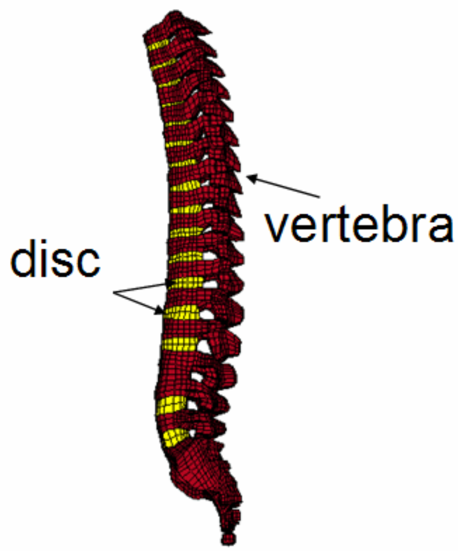

Figure 36 : Meshing of the vertebras and discs for 1YOC FE model

3.5.2.5 Meshing of the ribs and sternum

In this study, the ribs connect with the sternum by sharing nodes on the interface between rib and sternum. The sternum should be meshed by solid elements. Firstly, the shell elements were meshed on the surface of the sternum (Figure 3736a), and some lead lines were created on the lateral surface of the sternum based on the geometry. Based on the shell elements and lines, the sternum could be meshed by solid elements, as shown in Figure 3736b. By the same method, the shell elements covering the interface between rib cartilage and sternum were created (Figure 3736c). Creating lead lines based on the geometry of each rib, and then solid elements were created by dragging the shell elements along the lead lines (Figure 3736d). The whole skeleton of rib cage could be created by mapping the right part.

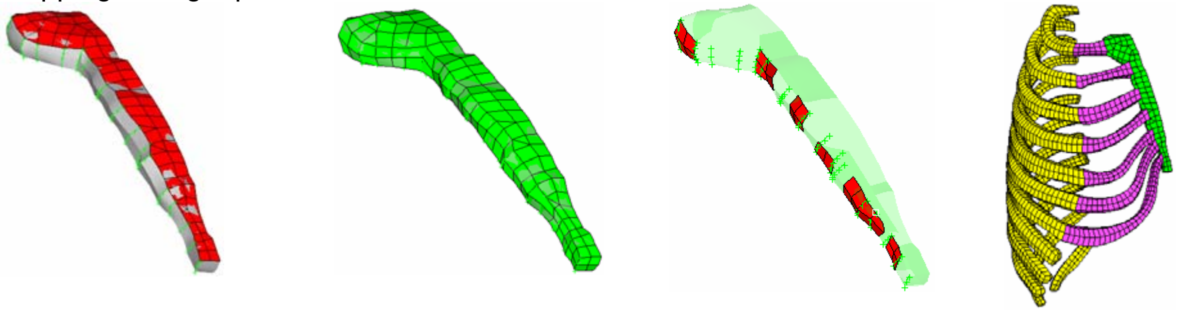

(a) (b) (c) (d)

Figure 37 : Meshing of the ribs and sternum

3.5.2.6 Meshing of the Scapula and pelvis

Scapula can be regarded as flat bone. The method of meshing the scapula bones is dragging of the shell elements which generated on the flat surface along the lateral geometry. As shown in Figure 3837a, the scapula was separated into two parts. Part 1 can be regarded as flat bone, the mesh layout was created by using shell elements firstly on the flat surface, as shown in Figure 3837b. Based on the shell elements, solid elements could be generated (Figure 3837c). By the same way, the part 2 could be meshed (Figure 3837d).

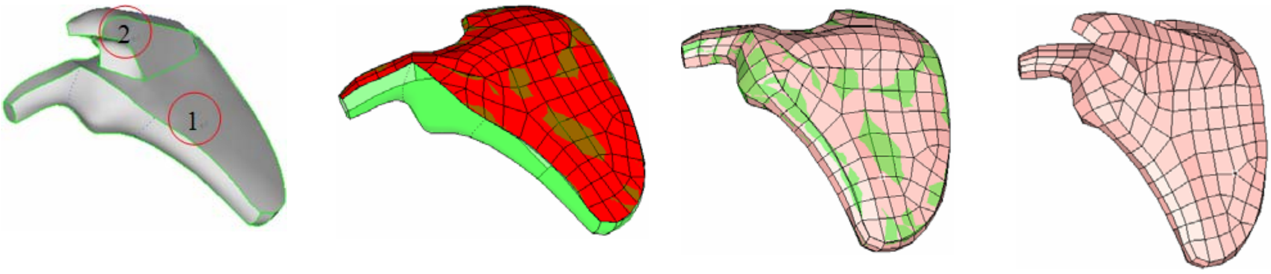

(a) (b) (c) (d)

Figure 38 : Meshing of the scapula

The shape of the pelvis is complicated relatively. The more parts should be divided (Figure 3938) for meshing. The way of meshing could be different for varying parts. Part 1 can be regarded as flat bone, the method is the same as that of scapula meshing. The method of re-mesh other four parts can refer to that of vertebra meshing.

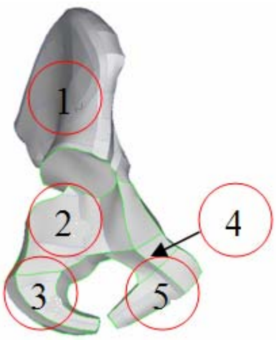

Figure 39 : The divided parts of pelvis for meshing

3.5.2.7 Meshing of the foot and hand

As shown in Figure 4039, the geometry of the bones on the foot and hand are in discrete manner. Each discrete part should be meshed respectively. The method is the same as mentioned above.

Figure 40 : Geometry of the foot and hand

3.5.2.8 Summary of mesh layout of whole skeleton model

The re-meshed whole skeleton was shown in Figure 4140, total element number is 54,931, and node number is 73,220.

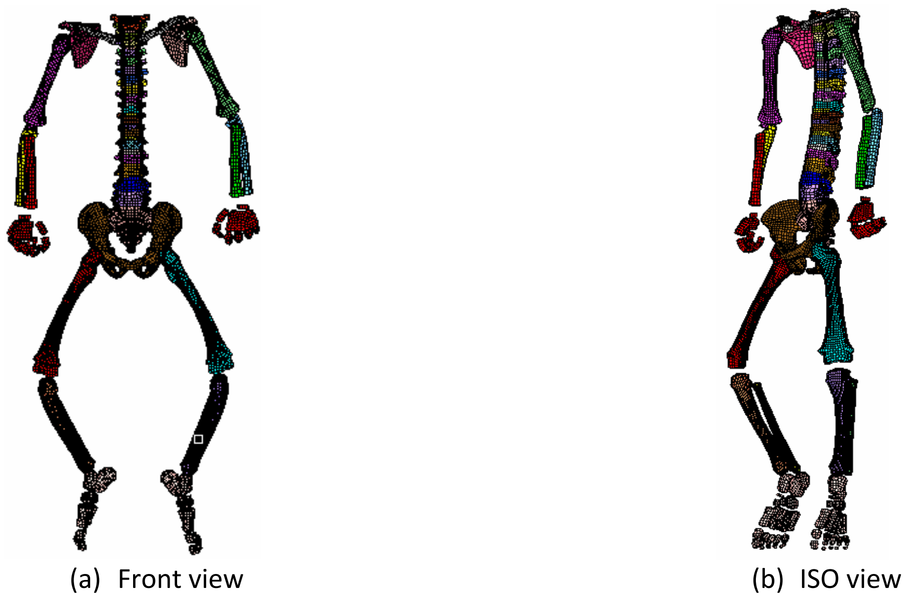

Figure 41 : Mesh layout of whole skeletons

3.5.3 Development of ligaments

The ligaments in the elbow joints, shoulder joints, hip joints, knee joints, and vertebras were developed when the model is regulated to the expectant anatomy position. As shown in Figure 4241, the tendons in the wrists, ankle joints, foot and hand were expressed by shell elements.

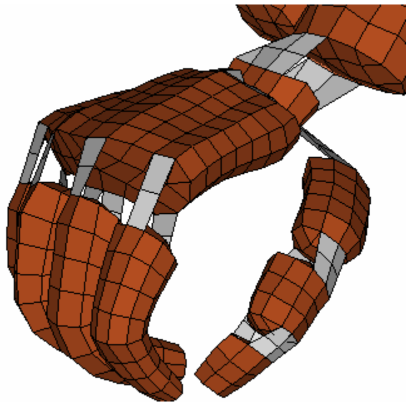

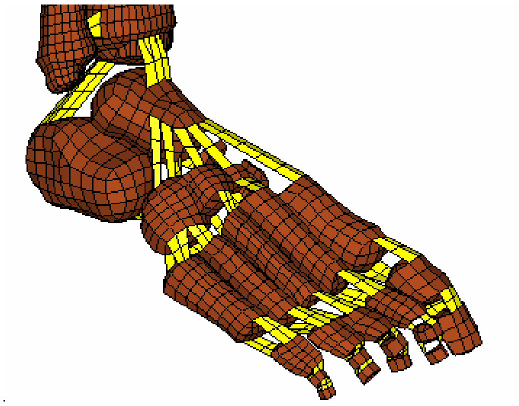

Figure 42 : Ligaments of wrists, hand, ankle joints and foot

3.5.4 Development of flesh

The flesh and skin were developed to wrap the remeshed skeleton. Surfaces of the skin were created based on the initial geometry information from STL files “skin-1YOC.stl”. As shown in Figure 4342, according to the characteristics of body segment anatomy structures, the whole skin was divided into four types of parts.

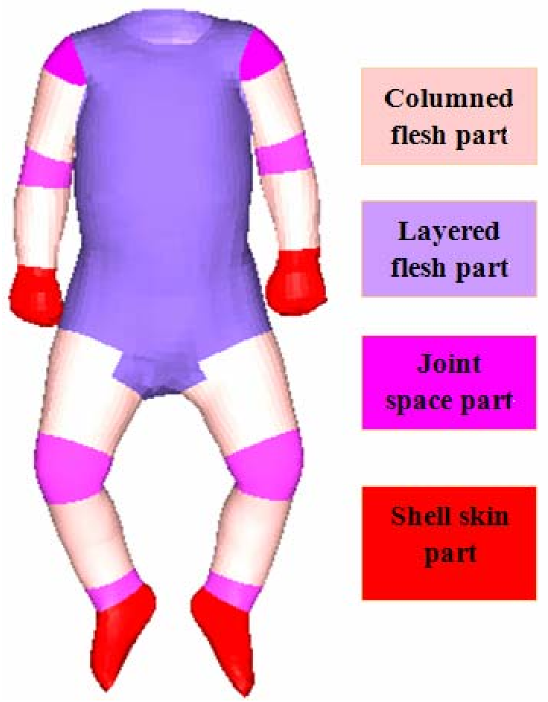

Figure 43 : Stratege for skin meshing

For the columned flesh part, a layer of shell elements covers the interface of long bone and flesh. A surface based on these shell elements and leading lines from the bone to the skin is created first, as shown in Figure 4443a, which formed a volume as a basis for meshing of the flesh of thigh by using solid elements as shown in Figure 4443b. By using the same method, other mesh laysout of columned flesh were generated.

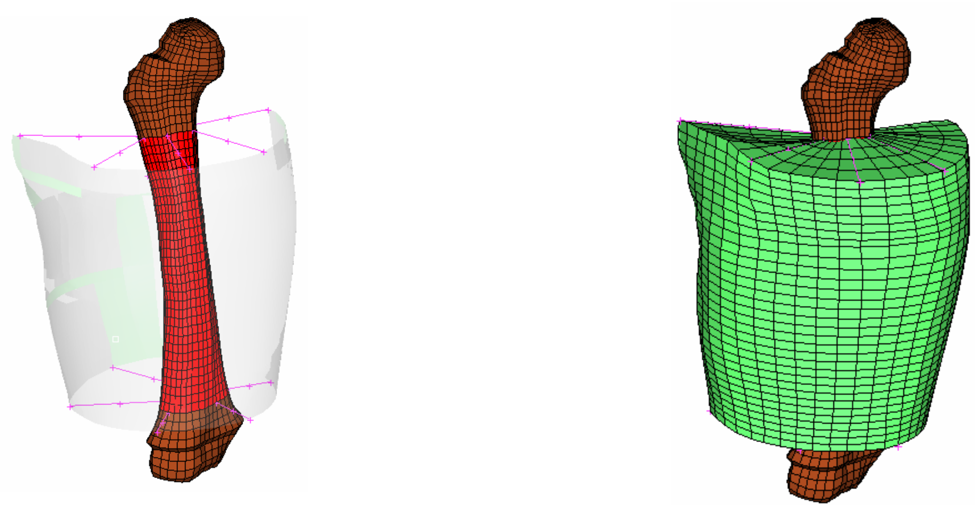

(a) (b)

Figure 44 : Remeshment of flesh of thigh

For the layered flesh part, only shell elements should be meshed on the skin surface (Figure 4544a). Then, the flesh was meshed by offsetting these shell elements for two layers, as shown in Figure 4544b.

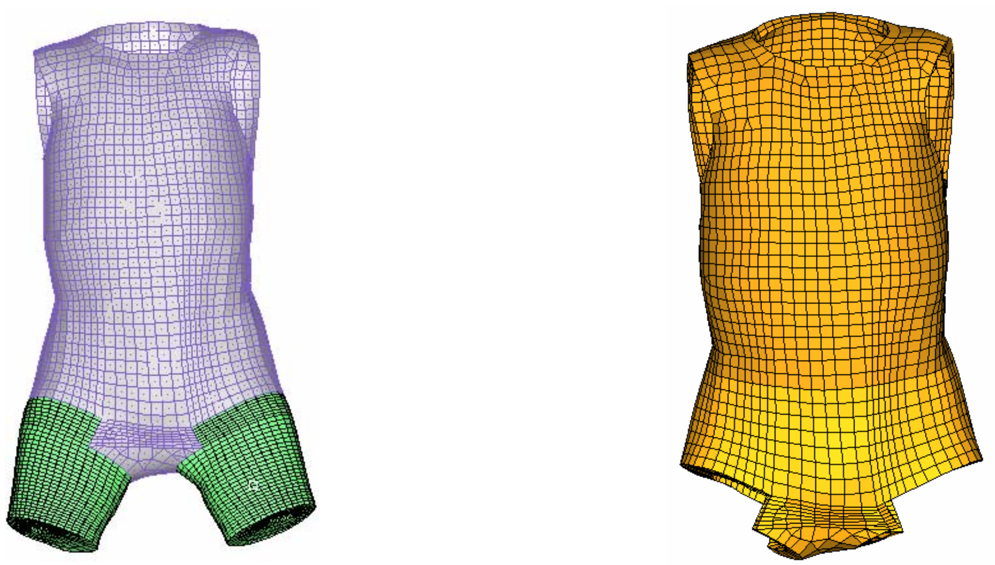

(a) (b)

Figure 45 : Remeshment of layered flesh

For Joint space part, only shell elements were created on the surface, and the flesh would be developed when the model is positioned to the expectant sitting posture. Only shell elements were meshed in the surface of Shell skin part.

3.5.5 Development of skin

The skin was modeled by using the shell elements. It was created on the segments of joint space, as well as the skin models that cover on the exterior surface of the flesh.

3.5.6 Conclusion

The developed model of the whole 1YOC body was shown in Figure 4645, total element number is 99,168, and node number is 110,753.

(a) (b)

Figure 46 : Developed 1YOC model

4 Conclusions

The objective of the present document, entitled deliverable D2.3.2 “report on 1Y and 6M child models”, is to present a 6 M.O.C. finite element head-neck model, a 6 month old multi-body full body human model as well as a one year old child finite element model developed in this project in terms of meshing segment per segment.

Head and neck finite element models of a 6 M.O.C have been development conducted by UdS as well as a 6 month old multi-body full body human model conducted by TNO.
The new finite element head model simulates closely the main anatomical features: skull, sutures, fontanel, falx, tentorium, subarachnoid space, scalp, cerebrum, cerebellum and brainstem.
Concerning the neck FEM, a simplified neck was developed just to reproduce a global behavior of this structure in terms of stiffness and mass.
For the 6 month old multi-body full body human model, as base model for the baby model, the TNO’s facet 50th percentile human occupant model was used and scaled down towards baby dimensions using the MADYMO/Scaler. The baby model geometry was based on CANDAT database geometry

The finite element model of 1YOC was developed by UdS. The other parts were developed by CHALMERS, including thorax, pelvis, upper limbs, and lower limbs.

The next step of this work consists to implement the mechanical properties in conformity with D2.2.2 results. After model validation and checking of model robustness where it is possible real world accident cases gathered from WP3 will be reconstructed numerically.
This accident simulation task will contribute to the model validation aspects as long as mechanical properties are concerned. These are the reason why definitive mechanical properties of child segment models are not included on the present deliverable.

After this phase of evaluation and adjustments, accidents cases (domestics and road) will be reconstructed in order started injury criteria development.

5 References

Duncan J.M. (1874):"On the tensile strength of the fresh adult fetus". British Medical Journal, Volume 19, pp. 763–4.

Jans G., Van-Audekercke R., Vander Sloten F., Gobin R., Van der Perre G., Mommaerts M.Y. (1998): "Bending properties of cranial bone segments of newborn children". 11th conference of the ESB, Toulouse, France.

Kallieris D., Barz J., Schmidt G., Heess G., Mattern R. (1976): "Comparison between child cadavers and child dummy by using child restraint systems in simulated collisions". Stapp Car Crash Conference, Paper No. 760815.

Koppens W.P. (1988): "The dynamics of systems of deformable bodies". PhD thesis, Eindhoven University of Technology, The Netherlands, 1988.

Luck J.F., Nightingale R.W., Loyd A.M., Prange M.T., Dibb A.T., Song Y., Fronheiser L., Myers B.S. (2008): "Tensile Mechanical Properties of the Perinatal and Pediatric PMHS Osteoligamentous Cervical Spine". Stapp Car Crash Journal, Vol. 52, November 2008.

MADYMO (2010a): MADYMO Theory manual v7.2. Delft, The Netherlands.

MADYMO (2010b): MADYMO Theory manual v7.2. Delft, The Netherlands.

McPherson G.K., Kriewall T.J. (1980): "The elastic modulus of fetal cranial bone: A first step towards an understanding of the biomechanics of fetal head molding". J Biomech. 1980, Vol. 13, pp. 9-16.

Ouyang J., Zhu Q., Zhao W., Xu Y., Chen W., and Zhong S. (2005): "Biomechanical Assessment of the Pediatric Cervical Spine Under Bending and Tensile Loading". J Trauma. 2006, Vol. 61, pp. 1492-1500.

Ouyang, J., Zhao W., Xu Y., Chen W., and Zhong S. (2006): "Thoracic Impact Testing of Pediatric Cadaveric Subjects". J Trauma. 2006;61:1492–1500.

Prange M.T., Luck J.F., Dibb A., Van Ee C.A., Nightingale R.W., Myers B.S. (2004): "Mechanical properties and anthropometry of the human infant head." Stapp Car Crash J., Vol. 48, pp. 279-99.

RAMSIS, RAMSIS Manual version 3.1, Tecmath Gmbh, Kaiserlautern, Germany, 1997.

Runge C.F., Youssef A., Thibault K.L., Kurtz S.M., Magram G., Thibault L.E.(1998):"Material properties of human infant skull and suture: experiments and numerical analysis". 9th Injury Prevention through Biomechanics Symposium, Detroit.

Twisk D. (1994): "Anthropometric data of children for the development of dummies", TNO report 750161275 Part 2, TNO Crash Safety Research Centre, Delft, The Netherlands.

Sandoz B., Vajda E., Alonzo F., Bruyère F., Bermond, F. (2011): "The mechanics of the in vivo infant and toddler trunk during respiratory physiotherapy". In press for journal Clinical Biomechanics, Elsevier.